Journal Name

ARTICLE TYPE

Cite this: DOI: 10.1039/xxxxxxxxxx

^{1}H NMR study of molecular order and dynamics in CBC9CB Liquid Crystal†

Alina Aluculesei,[a] Hugo Cachitas,[a] José Carvalho,[a] Fabian Vaca Chavez,[a] João L. Figueirinhas,[a] Pedro José Sebastião,[a#] Carlos Cruz,[a‡] Maria Gabriela Tamba,[b] Alexandra Kohlmeier,[b] and Georg H. Mehl[b]

Received Date
Accepted Date

DOI: 10.1039/xxxxxxxxxx

www.rsc.org/journalname

Molecular order and dynamics of the CB-C9-CB liquid crystalline dimer exhibiting the nematic (N) and the twist bend nematic (N_{tb}) phases were investigated by proton NMR spectroscopy, using fields of 0.78 T and 7.04 T, and relaxometry. The first relaxometry experiments for a very wide Larmor frequency domain (8 kHz - 300 MHz) on this system, using a combination of standard and fast field cycling NMR techniques, were performed. The spectroscopy results in the N_{tb} phase allowed us to probe the local molecular orientation relative to the N_{tb} helix axis. The relaxation data were analyzed considering order director fluctuations (ODF), molecular self-diffusion (SD) and local molecular rotations/reorientations (R) relaxation mechanisms. Global fits of theoretical relaxation models, as a function of temperature and Larmor frequency, for the phases under investigation, allowed for the determination of rotational correlation times, diffusion coefficients, viscoelastic parameters, correlation lengths and activation energies (in the case of thermally activated mechanisms). A clear difference between the structures of the N and N_{tb} phases was detected from the results of proton spin-lattice relaxation through distinct temperature and frequency dependencies' signatures of the collective modes. Significant pre-transitional effects were observed at the N-N_{tb} phase transition both from relaxometry and spectroscopy data. The experimental results correlate to data and models for comparable liquid crystalline systems.

1 Introduction

The nematic phase of liquid crystals is by far the most widely used in technological applications, of which the electro-optical displays are leaders in terms of economic impact. This fact, together with the scientific interest of this type of systems as fundamental soft matter phases, stimulates the search for nematic variants with novel physical properties, in particular if those are promising factors for industrial applications.[1] In 2010, a nematic-nematic phase transition was identified in a cyanobiphenyl dimer compound with an odd number of carbon atoms in the linking chain[2]. DSC measurements have shown that this was a weakly first order phase transition and the results of X-ray diffraction measurements on a two dimensional detector on both phases (below and above the N-N transition temperature) unequivocally identified the typical diffuse peaks corresponding to the lateral and longitudinal short range positional molecular ordering characteristic of the nematic phase[3,4]. Some authors have assigned the lower temperature nematic phase, occurring in similar compounds that exhibit this N-N transition, to the Nematic Twist Bend phase (N_{tb}), originally predicted by Meyer in 1973[5] and described by Dozov as a possible phase structure for bent-core mesogens in 2001[6]. In the N_{tb} phase, the molecules are positionally disordered and pack forming helicoidal structures, where each long molecular axis makes, in average, a tilt angle θ_t between 0° and 90° with respect to the nematic director. In some way, these systems would correspond to intermediate structures between the standard nematic phase with $\theta_t = 0°$ and the cholesteric phase with $\theta_t = 90°$[5]. The peculiar aspect of the dimers, that conjugate the eventual "bent-core" overall shape (in the case of the odd number of carbon atoms in the linking alkyl chain) with the global molecular flexibility allowed by the mobility of the aliphatic spacer is very likely at the origin of the emergence of the described N-N phase transition. At higher temperatures and sufficiently long spacers, increasing decoupling of the motions of the two linked rigid molecular segments (mesogenic groups) can occur, giving rise to

[a] Centro de Física e Engenharia de Materiais Avançados, Av. Rovisco Pais 1049-001 Lisbon, Portugal; Dept. of Physics, Instituto Superior Técnico, Universidade de Lisboa, Av. Rovisco Pais, 1049-001 Lisbon, Portugal
[b] Dep. of Chemistry, University of Hull, Cottingham Road, Hull, HU6 7RX, United Kingdom

† Electronic Supplementary Information (ESI) available: [details of any supplementary information available should be included here]. See DOI: 10.1039/b000000x/

‡ electronic address: carlos.cruz@tecnico.ulisboa.pt
# electronic address: pedro.jose.sebastiao@tecnico.ulisboa.pt

the classical uniaxial nematic phase. For lower temperatures, the odd number of carbons in the alkyl chain give rise to a molecular overall "twisted and bent" conformation associated with the "odd-even" effect, leading to the occurrence of a nematic with additional chiral ordering, even though the constituent molecules are achiral objects[4]. It was found that the molecular organisation in these structures is closely related to that found in crystalline systems determined in the bulk by XRD studies[7] or by the characterization of thin films using AFM techniques[8]. In recent years these systems have attracted the interest of different research groups both in theoretical and experimental terms, due to the mentioned fundamental and technological implications. In particular, the study of the flexoelectro-optic effect in these materials could open interesting paths for display applications[9,10]. Several studies on systems of this type, mostly on dimers with seven (CBC7CB)[4] or eleven (CBC9CB)[2] carbon atoms in the linking chain have been reported in the literature.

An alternative hypothesis for the molecular packing in the low temperature nematic phase exhibited by these dimer systems was also presented in the literature[11]. According to that model, based on ^{2}H NMR spectroscopy results obtained with selectively deuterated molecules, the molecules in that phase (labeled N_x) are packed into small local chiral clusters with opposite chiralities, but defining a single long range uniformly oriented director and not the long range helicoidal arrangement proposed for the N_{tb} phase.

More recently, studies of resonant X-ray diffraction gave evidence of the chiral arrangement in the N_{tb} phase of CBC7CB[12] and similar compounds[13], allowing for the measurement of an helical pitch of the order of 10 nm or, in other words, of two or three molecular lengths.

Proton NMR relaxation is an experimental technique particularly useful for the study of molecular dynamics, especially when the results are obtained over large Larmor frequency domains, revealing the corresponding wide range of molecular movements timescale. As the molecular motions are conditioned by the phase structure of liquid crystalline systems, this technique also provides an important insight to the different forms of molecular organization in the studied mesophases. Besides molecular rotations/reorientations and self-diffusion that are particularly sensitive to the local molecular arrangements, the detection of collective movements, typical of liquid crystalline systems, are specially useful to the mesophases structural characterization, since this mechanism is mostly determined by the long range molecular disposition[14]. Collective movements are normally slow (comparing with molecular self-diffusion and local rotations/reorientations) dominating, in general, the Larmor frequency dispersion of the NMR T_1 relaxation rates from the kHz to a few MHz domain. In the work presented herein, T_1 proton NMR relaxation data were obtained, for the compound CBC9CB, as a function of the Larmor frequency, from 8 kHz to 300 MHz, and of temperature in the isotropic liquid and nematic phases exhibited by the compound. The wide frequency range was scanned using a combination of standard and fast field-cycling NMR[15] as described in the experimental section of the paper. Additionally, proton NMR spectra were obtained for high (7.04 T) and low (0.78 T) static magnetic fields in the temperature range of the two nematic phases exhibited by the system. As will be shown ahead, both the NMR relaxation and spectroscopy data put into evidence a clear distinction, between the two nematic mesophases, that will be discussed taking into account the information present in the literature. This work was carried out aiming to contribute to the interesting discussions on the physical properties of the new found nematic phase and its molecular organization.

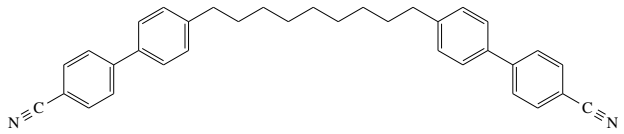

Ntb $\rightarrow$ 380.1 $\pm$ 0.2 K Nu $\rightarrow$ 395.7 $\pm$ 0.2 K Iso
Iso $\rightarrow$ 395.3 $\pm$ 0.2 K Nu $\rightarrow$ 379.5 $\pm$ 0.2 K Ntb

Fig. 1 Structure of the CB-C9-CB molecule. Phase sequence obtained using polarising optical microscopy, POM.

2 EXPERIMENTAL

The material under investigation in this work is the liquid crystal dimer commonly referred as CBC9CB, composed by two cyanobiphenyl rigid mesogenic units linked by a flexible alkyl chain with 9 carbon atoms. Actually, the CBC9CB molecule can be described as a dimer composed by two monomers identical to 5CB, sharing the terminal carbon atom. The sample used was synthesized in the Chemistry Department of the University of Hull, UK,[3].

The molecular structure and phase sequence of the compound are presented in FIG. 1. The recorded transitions temperatures detected by polarizing optical microscopy are in good agreement with those presented in[3] and[16].

The NMR studies were carried in a vacuum sealed CBC9CB sample using a 5mm outer diameter standard NMR tube. Proton NMR spin-lattice relaxation data and spectra were collected over the temperature range from 406 K to 355 K covering the N and N_{tb} mesophases of the LC coumpound. The spectra were collected using a Bruker Avance II 300 MHz NMR spectrometer connected to either a superconducting magnet for the high field spectra or a BE30 variable field electromagnet for the low field spectra. These spectrometers were also used to measure the proton spin-lattice relaxation data, T_1, in the Larmor frequency (ν_L) range , 10 MHz-300 MHz. In addition, a home-developed fast field-cycling (FFC) NMR relaxometer was used to obtain the experimental values of T_1 for frequencies below 10 MHz and above 8 kHz.

2.1 Proton NMR Spectroscopy, experimental details

The absortion spectra were obtained using a 90° pulse width of 6μs. The recyling delay was set at 4s. For each temperature 256 free induction decay signals, FIDs, were recorded. The temperature was regulated to 0.2K resolution and the estimated temperature gradient over the sample volume falls bellow 0.6K.The sample was initially taken to the isotropic phase and then slowly cooled inside the magnet to the selected temperatures where it was left for a equilibration delay of up to 600 s before data acqui-

sition.

2.2 Proton NMR Relaxation

The T_1 measurements for frequencies above 10 MHz were made using the conventional inversion-recovery radio-frequency pulse sequence with phase cycle to remove DC bias. Since the signal-to-noise ratio is basically proportional to $B^{3/2}$ [15] ($B = 2\pi\nu_L/\gamma_H$) this experimental technique can not be used, in practice, for fields below 0.2 T ($\sim$ 9 MHz for ^{1}H). Fast field-cycling can circumvent this problem by submitting the sample to different magnetic field values during a measure cycle (typically two different magnetic field values). In the most common FFC cycle the sample is left to stabilise its nuclear magnetization at magnetic polarisation field B_P, then submitted to a lower magnetic field value, B_E, during a variable/adjustable time τ, and finally submitted again to a higher magnetic field B_D for detection of the magnetisation value, by applying a $\pi/2$ r.f. pulse. In most cases $B_D = B_P$. The advantage of this experimental technique lies in the fact that the FID signal detected can provide information about the nuclear magnetisation value after time τ, which depends on the value of B_E and $T_1(B_E)$, but its strength depends on the value of B_D [15]. In this way T_1 can be measured for different B_E values using always the same B_D as the FID detection field.

All measurements were made after cooling the sample from the isotropic phase to the desired temperature at a cooling rate of 1°/min.

3 RESULTS AND DISCUSSION

3.1 Proton NMR Spectroscopy in the N and N_{tb} phases

The molecular organization in the N_{tb} phase is still being discussed and NMR spectroscopy can bring a relevant insight into the problem. Several NMR studies on the N_{tb} phase have been carried out using different compounds including CBC7CB [4,17,18], CBC9CB [11,19–21], and others [22]. These studies have used either deuterium and/or carbon 13 and have established that the high temperature nematic and the N_{tb} phases are both uniaxial and the N_{tb} phase shows enantiotopic discrimination [4,11,23], in the N_{tb} phase the two hydrogens of the first methylene bridges in the chain become inequivalent. L. Beguin et al. [17] showed further that this property extends to all methylene bridges except the central one in the dimers' chain. This fact was attributed to the onset of a chiral molecular arrangement in the N_{tb} phase due to the increase bent conformation of the molecules. The residual C-H dipolar interaction study of Emsley et al. [18] nevertheless claims that on going from the N to the N_{tb} phase the molecular conformation landscape is not significantly altered. In this work we have analyzed the hydrogen spectra in both the N and the N_{tb} phases of the compound CBC9CB at two distinct Larmor frequencies 300MHz and 33.4MHz corresponding to the fields of 7T and 0.78T respectively. The spectra are dominated by the dipolar interaction and in the N phase are composed of two broad peaks approximately centered at the resonance frequency and showing some internal structure as can be seen in figures 2 and 3.

This indicates that in the N phase at both fields the nematic director is well aligned by the magnetic field. In the N_{tb} phase at low field the spectra show a powder pattern indicating that a distribution of domain orientations is present in the sample. This observation is compatible with polarizing optical microscopy studies that show a non uniform director arrangement with a characteristic texture in the N_{tb} phase. At 7 Tesla, the ^{1}H spectra in the N_{tb} phase are similar to those in the N phase, showing that the high magnetic field strength prevents the onset of the type of domain orientation distribution seen at low field in the N_{tb} phase as supported also by other high field NMR studies in this phase [4,11].

The high field proton NMR spectra of figure 2 also show that for T = 398 K the CB-C9-CB compound is in the nematic phase, while the I-N transition temperature detected by polarized optical microscopy is around 395K. The magnetic field induced I-N transition temperature increase in this and other dimer systems has already been reported in the literature [24].

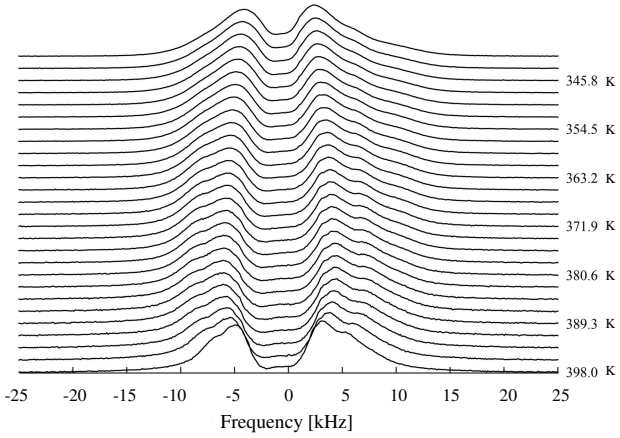

Fig. 2 Stack plot of high field proton spectra in the N and N_{tb} phases

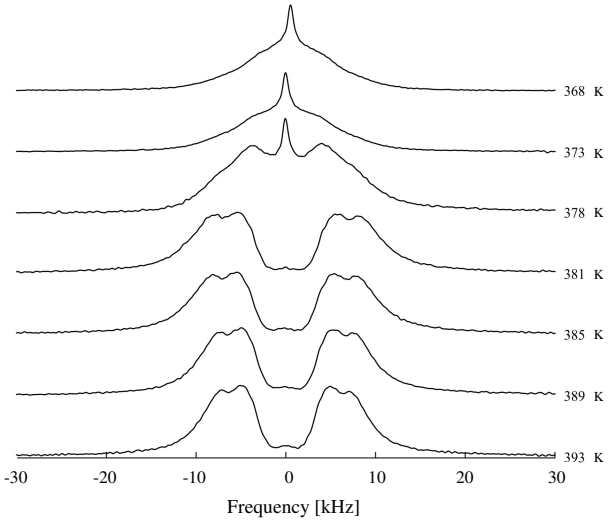

Fig. 3 Stack plot of low field proton spectra in the N and N_{tb} phases

3.1.1 Model, Results and Discussion

Following the temperature evolution of the high field proton spectra in the N and N_{tb} phases shown in figure 2 one observes that the shape of the spectra does not change significantly, as the temperature decreases in the N phase the splitting between the large lobes increases while within the N_{tb} phase range it decreases. This temperature evolution can then be quantified by a single temperature dependent parameter $A(T)$ which gives the contraction/expansion factor of the frequency scale of each spectrum relative to a reference spectrum. This behaviour of the proton spectra can be understood recalling that in anisotropic liquid crystalline phases the high field proton NMR spectra is dominated by the direct dipolar interaction between pairs of protons. This interaction being anisotropic, is linearly dependent on the molecular order parameters which are temperature dependent quantities. Under appropriate conditions this interaction may become approximately proportional to a single temperature dependent order parameter as detailed next. The direct dipolar interaction between pairs of protons falls off with distance between protons as $1/r^3$ and as the molecules are expected to diffuse rapidly in the LC phases under study, the relevant dipolar interactions for each proton are those with the nearest neighbours in the same molecule. Besides the high magnetic field proton NMR spectra can be calculated in first order perturbation theory considering the dipolar interaction averaged over the fast molecular motions as a perturbation to the Zeeman Hamiltonian. The indirect spin coupling and the chemical shift can safely be neglected in our approximate analysis. The time averaged direct dipolar coupling Hamiltonian $\overline{H_D}$ is given by:

$$\overline{\mathscr{H}}_D = \frac{\mu_0}{4\pi}\gamma^2\hbar^2 \sum_{k=1,l>k}^{N-1,N} \left\{ \left[I_{k,Z}I_{l,Z} - \frac{1}{4}\left(I_{k,+}I_{l,-} + \right.\right.\right.$$
$$\left.\left.\left. + \; I_{k,-}I_{l,+}\right)\right] \overline{\left[\frac{1}{r_{kl}^3}\left(1 - \frac{3}{r_{kl}^2}r_{kl,Z}^2\right)\right]} \right\}. \quad (1)$$

where γ is the gyromagnetic ratio for protons, $I_{k,i}$ is ether the Z component ($i = Z$) of the spin operator for spin k or the lowering or raising operators for that spin ($i = +, -$), N is the number of interacting spins in each molecule,r_{kl} is the distance between spins k and l, $r_{kl,Z}$ is the Z component of the vector joining spin k to l and the Z axis is defined by the static B_0 field. The proton spectra is determined by this Hamiltonian term with the spectral resonance lines arising from the transitions between the Hamiltonian energy levels. The quantities $F_{kl}^{ZZ} \equiv \overline{[1 - 3\left(r_{kl,Z}/r_{kl}\right)^2]/r_{kl}^3}$ are the ZZ components of second rank traceless symmetric tensors in the laboratory frame and they are proportional to the line splittings in the proton spectra. For the cases of monodomain samples in the N phase with the director parallel to the B_0 field and in the N_{tb} phase with the helix axis parallel to the B_0 field and when the pair of spins involved belongs to the same 'ith' rigid molecular segment, it is possible to express these ZZ tensor components in the lab. frame as functions of the Saupe order tensor for that rigid molecular segment. The relations are given by 2, with the Saupe order tensor defined by $S_{i,\alpha\beta} \equiv \left\langle \frac{3}{2}\cos\theta_{Z\alpha}\cos\theta_{Z\beta} - \frac{1}{2}\delta_{\alpha\beta}\right\rangle$ where α, β refer to a chosen molecular segment frame axis (x,y,z). $\langle\rangle$ indicates an ensemble average and the molecular segment defined tensor components $F_{kl}^{m,\alpha\beta}$ are given by $F_{kl}^{m,\alpha\beta} \equiv \left[\delta_{\alpha,\beta} - 3r_{kl,\alpha}r_{kl,\beta}/r_{kl}^2\right]/\left\langle r_{kl}^3\right\rangle$, where $\left\langle r_{kl}^3\right\rangle$ indicates an average over local vibrations.

$$F_{kl}^{ZZ} = S_{i,zz}F_{kl}^{m,zz} + \frac{1}{3}\left(S_{i,xx} - S_{i,yy}\right)\left(F_{kl}^{m,xx} - F_{kl}^{m,yy}\right)$$
$$+ \frac{4}{3}\left(S_{i,xy}F_{kl}^{m,xy} + S_{i,xz}F_{kl}^{m,xz} + S_{i,yz}F_{kl}^{m,yz}\right). \quad (2)$$

The tensor $S_{i,\alpha\beta}$ can be diagonalized and in its principal frame where on average the Z axis will be parallel to its z axis ($\langle e_Z^{\rightarrow}\rangle = e_z^{\rightarrow}$), equation 2 takes the form:

$$F_{kl}^{ZZ} = S_iF_{kl}^{m,zz} + D_i\left(F_{kl}^{m,xx} - F_{kl}^{m,yy}\right)/3, \quad (3)$$

where $S_i \equiv S_{i,zz}$ and $D_i \equiv \left[S_{i,xx} - S_{i,yy}\right]$ are respectively the nematic order parameter and the molecular biaxiality parameter for that rigid molecular segment. Considering now that the most ordered molecular segments in a nematic phase (those with highest S), coinciding in general with the mesogenic groups, will have their bounded hydrogens contributing mostly to the widest split lines in the NMR spectra, one finds that for those segments while S has the largest values, D is in general small making F_{kl}^{ZZ} approximately directly proportional to the order parameters S_i and $F_{kl}^{m,zz}$ as

$$F_{kl}^{ZZ} = S_iF_{kl}^{m,zz} = -2S_iP_2(cos\beta_{kl,z})/ < r_{kl}^3 >, \quad (4)$$

where P_2 represents the second degree Legendre polynomial and $\beta_{kl,z}$ is the polar angle of the kl inter-proton axis in the (x,y,z) molecular segment principal frame of $S_{i,\alpha\beta}$. Using the addition theorem for spherical harmonics 4 can further be written as

$$F_{kl}^{ZZ} = -2S_i[P_2\left(cos\beta_{z,z_1}\right)P_2\left(cos\beta_{kl,z_1}\right) + g]/ < r_{kl}^3 > . \quad (5)$$

where z_1 is a selected molecular segment fixed axis. The extra terms represented by g are neglectable if β_{z,z_1} and/or β_{kl,z_1} are not large. In that case 5 takes a form that can be useful;

$$F_{kl}^{ZZ} = -2S_iP_2(cos\beta_{z,z_1})P_2(cos\beta_{kl,z_1})/ < r_{kl}^3 > . \quad (6)$$

This form gives rise to absorption lines whose splittings scale linearly with the S_i and $P_2(cos\beta_{z,z_1})$ and if the S_i all bare similar temperature dependencies and the eventual reorientation of the principal frames with temperature results in a common change of the factors $P_2(cos\beta_{z,z_1})$ for the different molecular segments, the line shape will be unaffected by temperature, only the line splitting will change as approximately found in our system. The remaining dipolar Hamiltonian contributions arising from the spin interactions between non rigidly fixed spins are also linear in the order parameters associated with each molecular conformer but depend also upon the molecular conformational landscape displaying a potentially more complex behaviour on the temperature. In face of the experimental results the former contributions

seem to dominate over the last ones in this system. Equation 6 shows that the tensor components F_{kl}^{ZZ} defining the line splittings in the hydrogen spectra depend linearly upon both the order parameter S_i and a orientation dependent parameter $P_2(cos\beta_{z,z_1})$ for each molecular segment. The molecular z_1 axis may be conveniently chosen as a relevant molecular axis as for instance the para axis of the benzene rings of the mesogenic units. In this way β_{z,z_1} represents the tilt of the mesogenic units relative to the Z axis.

The high field spectra were then analysed comparing them to the selected reference spectrum recorded at T=385K. The spectra were fitted to the expression

$$G(\omega) = BG'\left(\frac{\omega-\omega_0}{A}\right) \quad (7)$$

where $G'(\omega)$ is the chosen reference spectrum. A, B and ω_0 are fitting parameters. Fitted spectra at specific temperatures are shown in figure 4. While the quality of the fits is very good at the highest temperatures it drops quite a bit at the lowest ones in the N_{tb} phase showing that some of the hypothesis behind the frequency scaling model are not so good approximations at these lower temperatures. The temperature evolution of parameter A is shown in figure 5 along with a fit using a model described below. B and ω_0 are a scaling and a frequency shift parameter that vary slightly from spectra to spectra. In view of the quantities F_{kl}^{ZZ} defining the spectral line splittings and their relation with both the order parameters S_i and the orientation parameters $P_2(cos\beta_{z,z_1})$ it is reasonable to expect the parameter A to depend linearly upon both an average molecular order parameter S and an average molecular orientation parameter $P_2(cos(\beta))$. $A(T)$ closely matches the broad line splitting of the proton spectra as it should, A increases as T decreases in the N phase and then close to the N-N_{tb} phase transition A starts to decrease with decreasing T. The increase of A within the most T range of the N phase goes along with the expected increase in the nematic order parameter S when T is lowered, but the decrease of A within the N_{tb} phase as T decreases indicates most probably an increase in the tilt angle of the molecular segments relative to the helix axis (coinciding with the Z axis introduced above) in this phase as T goes down since a decrease in order in the N_{tb} phase is not expected. To account for these effects the parameter A is modelled as follows;

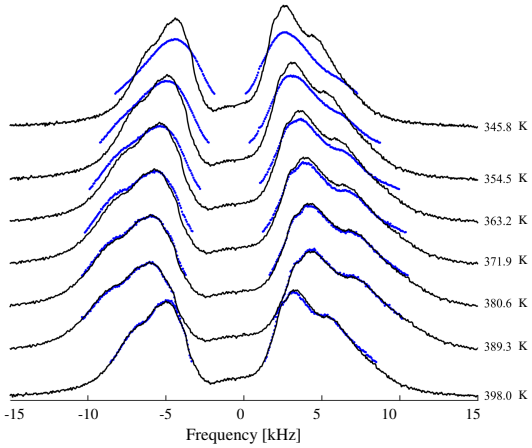

Fig. 4 Stack plot of high field proton spectra and fits in the N and N_{tb} phases

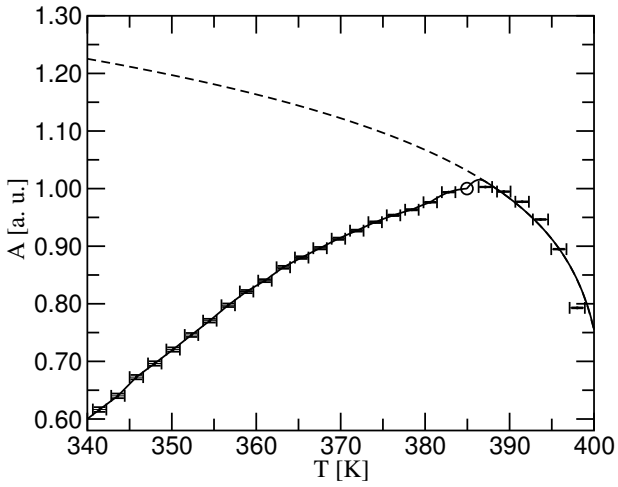

Fig. 5 Temperature dependence of A along with the model fit covering the N and N_{tb} phases range.The solid curve corresponds to the fitting curve (8). The dashed curve represents the fitting curve (8), keeping $\beta(T) = \beta_r$ at all temperatures.

$$A(T) \propto S(T)\frac{P_2[\cos\beta(T)]}{P_2(\cos\beta_r)}. \quad (8)$$

where $S(T)$ represents an average order parameter for the mesogenic groups mainly, as they are expected to be the most ordered molecular segments and their proton pairs those mostly responsible for the large spectral lobes recorded.[?] β represents an average angle between a chosen significant axis in each mesogenic unit (as the para-axis of the benzene rings) and the most ordered molecular axis for that unit. The average orientation of the most ordered axis coincides with either the director in the N phase or the helix axis in the Ntb phase. The average orientation of the mesogenic units can be associated with the local director considered in the model of the Ntb phase. β_r is the value of $\beta(T)$ in the N phase assumed to be constant down to the temperature of the maximum value of $A(T)$. Below that temperature and within the N_{tb} phase, $\beta(T)$ must increase with the decrease in T to match the experimentally observed evolution of $A(T)$ and excluding a non expected decrease in the order parameter $S(T)$. Defining $\Delta\beta = \beta(T) - \beta_r$, $A(T)$ can be further simplified when $\Delta\beta$ is not large, leading to

$$A(T) \propto S(T)P_2[\cos(\Delta\beta(T))] = \\ = S_0\left(1-\frac{T}{T^*}\right)^{\alpha} P_2[\cos\Delta\beta(T)] \quad (9)$$

where $S(T)$ is modelled by the Haller law[25] with parameters S_0, T^* and α. Due to the limited number of NMR fitting points in the N phase, S_0 and T^* were taken as fitting parameters and

$\alpha = 0.1326 \pm 0.0010$ was obtained by fitting the birefringence data reported in [26] to the Haller law. In this approach, $S(T)$ introduced in Equation 8 is mainly the order parameter for the mesogenic groups relative to the director in the N phase and the helix axis in the N_{tb} phase. In other studies of order in the N_{tb} phase [20,27,28] the molecular segments' order is also defined relative to a local director which according to the proposed helical structure for the N_{tb} phase [4,5] is tilted relative to the helix axis. This tilt angle describing in average the tilting of the molecular segments relative to the symmetry axis of the helical structure identifies a similar tilt as the angle β introduced above, regardless of the fact that the two angles are defined in different frames, β appearing in Equation 8 is defined in the molecular segment fixed frame while the helical structure tilt is defined in the phase frame. Figure 5 shows $A(T)$ and the model fit. From the fit we obtained $\Delta\beta(T)$ shown in figure 6 and S_0 is absorbed in the proportionality constant of A.

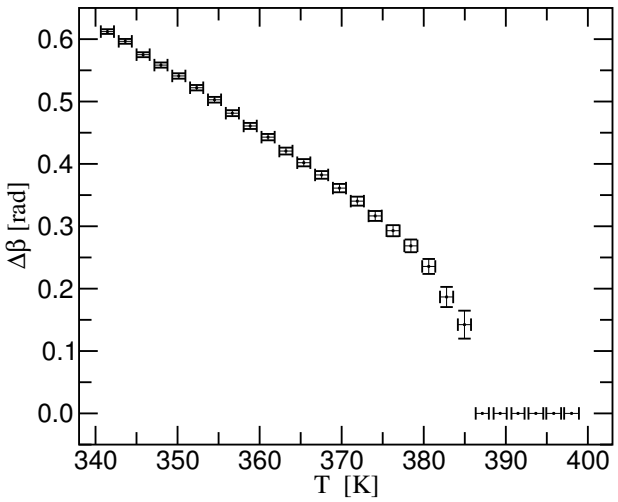

Fig. 6 Temperature dependence of $\Delta\beta$ obtain from the fit of $A(T)$ covering the N and N_{tb} phases range.

At the higher temperatures, $\beta(T)$ is considered to be temperature independent, and, therefore, $\Delta\beta = 0$. In the low temperature range of the N_{tb} phase, the steady increase of $\Delta\beta$ with decreasing temperature may be overestimated due to extrapolation with the Haller law far from the I-N phase transition. Nevertheless, the values obtained for $\Delta\beta$ are in line with those reported in the literature for similar systems [20,22].

The temperature dependence of $\Delta\beta(T)$ shows an increased tilting of the molecular axis as T decreases starting before the onset of the N_{tb} phase and continuing in this phase, compatible with and increasing average bent conformation of the molecule, while the value of α is slightly lower than other nematics, [25], in which $\alpha \sim 0.18$. It is also noteworthy to point out that below the temperature of the maximum of $A(T)$ $\Delta\beta$ increases approximately linearly with decreasing temperature in both N and N_{tb} phase ranges. However after the onset of the N_{tb}, at approximately $T = \sim 380$K, the slope of this linear behaviour seems to decrease.

Comparing our results on the angle $\Delta\beta$ to those of reference [20], where orientational order in the CBC9CB compound was also studied, we verify that our values for $\Delta\beta$ are close to those obtained in [20]. However the pre-transitional increase in $\Delta\beta$ detected in our study is not observed in [20], and also $\Delta\beta$ is slightly larger than the tilt reported in [20], in average by as much as $\Delta\beta$ at the transition N_{tb}-N. The reasons for the discrepancy found may be twofold. Firstly both results rely heavily on the validity of the Haller law extending from the N to the N_{tb} phase what may be questionable due to the nature of the N_{tb} phase. Secondly, different molecular probes were used to obtain the tilt angles. Even though, the values of $\Delta\beta$ obtained herein are also in line with those reported for similar systems [22]. Considering now the low field spectra, it is found that in the N phase the spectra are similar to the high field spectra but in the N_{tb} phase they are quite different indicating that the sample departs from a monodomain on entering the N_{tb} phase. To account for these spectra a distribution of domain orientations must be taken into account with each nematic domain contributing to the spectra with a term of the form

$$G(\omega,\theta) = \frac{G'\left(\frac{\omega}{\left|\frac{3}{2}\cos^2\theta - \frac{1}{2}\right|}\right)}{\left|\frac{3}{2}\cos^2\theta - \frac{1}{2}\right|} \quad (10)$$

where θ is the angle between the magnetic field and each nematic domain symmetry axis. $G'(\omega')$ is given by 7 with $A(T)$ obtained from the high field spectra analysis. Expression 10 is singular for theta equal to the magic angle, as the simple frequency scaling used does not include the finite line width of the spectral lines, to overcome this shortcoming, 10 must be convoluted with a line shape function. The spectra is calculated adding up the contribution from all domains, each one weighted by the domain orientation distribution function leading to

$$G(\omega) = \int_0^{\pi}\int_{-\infty}^{\infty} \frac{G'\left(\frac{\omega-\omega'}{\left|\frac{3}{2}\cos^2\theta - \frac{1}{2}\right|}\right)}{\left|\frac{3}{2}\cos^2\theta - \frac{1}{2}\right|} h(\omega',\Delta) f(\theta)\sin\theta d\theta d\omega' \quad (11)$$

where a normalized lorentzian line shape was used,

$$h(\omega',\Delta) = \frac{1}{2\pi}\frac{\Delta}{\omega'^2 + \frac{\Delta^2}{4}}. \quad (12)$$

The domain orientation distribution function $f(\theta)$ is parametrized in terms of a series expansion of even Legendre polinomials up to order 10 and requiring that $f(\theta) \geq 0$, $f(\theta) = max\left[\sum_{i=0}^{i=5} a_{2i} P_{2i}(\cos\theta), 0\right]$. The coefficients of the series expansion and ω_0 appearing in Equation 7 are the fitting parameters. The spectra at low fields along with the fits are shown in figure 7.

The domain orientation distribution function in the N_{tb} phase appears in figure 8 where it can be seen that the domain symmetry axis orientations are more concentrated around 0 and π with a smaller contribution from orientations around $\frac{\pi}{2}$.Additionally, the

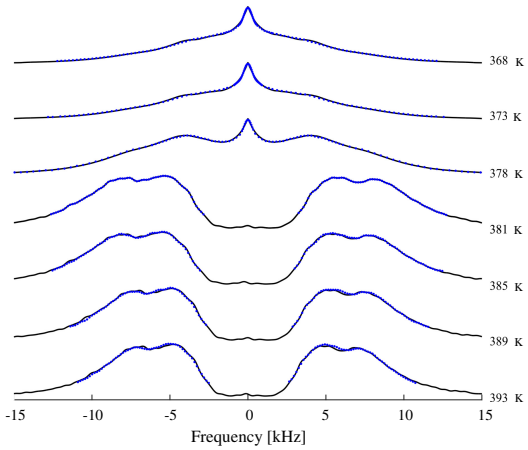

Fig. 7 Stack plot of low field proton spectra and fits in the N and N_{tb} phases

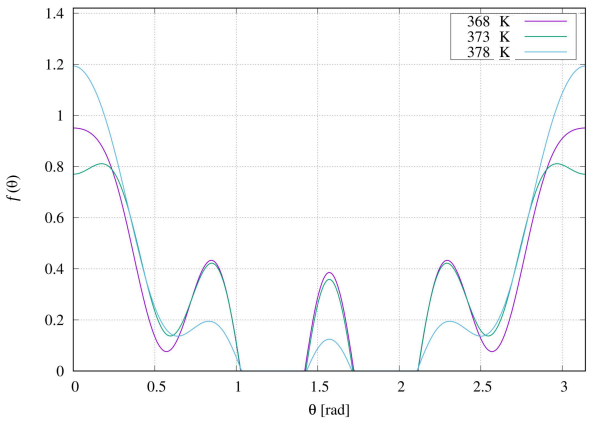

Fig. 8 Domain orientation distribution function in the N_{tb} phase obtained from the fitting of the low field spectra

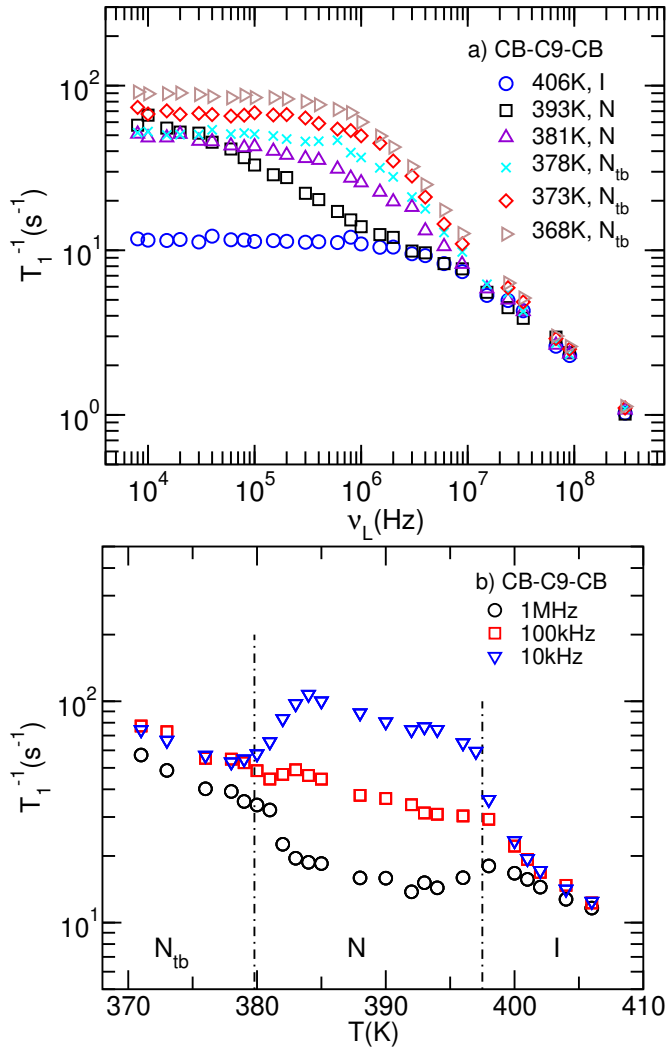

Fig. 9 (Color online) CB-C9-CB experimental spin-lattice relaxation results as a function of the Larmor frequency and temperature. a) T_1^{-1} as a function of the frequency for different temperatures; b) T_1^{-1} as a function of temperature. The dashed lines correspond to the transition temperatures indicated in figure 1.

contribution from the orientations around $\frac{\pi}{2}$, seems to increase with decreasing temperature, while the predominant contribution from the orientations concentrated around 0 and π exhibits the opposite behavior.

3.2 Proton T_1 Results and Discussion

3.2.1 Experimental data

As previously referred, proton NMR relaxation is a valuable tool for the analysis of molecular dynamics in LC phases and, with particular emphasis in the case of collective movements, a helpful resource contributing to the understanding of the mesophases' structural properties. In order to attain, as much as possible, a comprehensive experimental approach, it is useful to collect relaxation data both as a function of temperature (for the phases under investigation) and Larmor frequency (dispersion curves). The joint analysis of both the temperature and frequency dependence of the ralaxation times, using global fits of NMR relaxation theoretical models for the different mesophases, generally provides a consistent interpretation of the physical properties under investigation. The experimental spin-lattice relaxation rate T_1^{-1} results obtained in this study are presented in figure 9. The T_1^{-1} dispersion results are presented in figure 9-a) for temperatures 406, 393, 381, 378, 373, and 368 K covering the three phases investigated: isotropic, I, nematic, N, and twist-bend nematic phase, N_{tb}, respectively. In figure 9-b) the values of T_1^{-1} are presented as a function of temperature for three selected frequencies: 1 MHz, 100 kHz, and 10 kHz, respectively.

As it can be observed in figure 9-a) the T_1^{-1} dispersion is clearly different in the nematic phase in comparison with the isotropic phase for frequencies below 20 MHz. As temperature decreases, the T_1^{-1} dispersion changes and a frequency plateau starts to appear, first below 100 kHz at 381 K, then below 1 MHz at 368 K.

The differences in the dispersion profiles can also be observed in the temperature figure 9-b). The I-N transition is clearly perceived in this figure, in particular at the 10 kHz frequency. The T_1^{-1} at 10 kHz presents strong variations in the temperature range

associated with the classical nematic phase. In this temperature range T_1^{-1} increases with decreasing temperature until 384 K and then decreases with decreasing temperature until the N-N_{tb} transition temperature. The I-N and N-N_{tb} phase transitions can also be perceived at 100 kHz and 1 MHz but the changes in the T_1^{-1} profile are less expressive.

The spin-lattice relaxation dispersion in the isotropic phase presents the typical low dispersion for frequencies below 10 MHz already seen in many isotropic phases of liquid crystals including 5CB[29]. The T_1^{-1} dispersion in the N phase at 393 K is also similar to that observed for the nematic phase of 5CB[29]. However, the dispersions obtained for temperatures between 381 K and 368 K present low frequency plateaus that extend to unusual high frequencies when compared with other nematic phases[29,30].

3.2.2 Model fits

The experimental T_1^{-1} were analised taking into account a relaxation model that includes local molecular rotations/reorientations, R, translation self-diffusion, SD, and order-director fluctuations, ODF. Assuming that the correlation times for these molecular motions are clearly different and/or the molecular motions are statistically independent or otherwise the fluctuations of dipolar spin interactions are spatially restricted in different conditions

$$\frac{1}{T_1} \simeq \left(\frac{1}{T_1}\right)_{\mathrm{R}} + \left(\frac{1}{T_1}\right)_{\mathrm{SD}} + \left(\frac{1}{T_1}\right)_{\mathrm{CM}} \tag{13}$$

and cross-relaxation terms can be neglected as a first approximation. CM stand for collective motions that are order director fluctuations, ODF, in the nematic phases and order parameter fluctuations, OPF, in the isotropic phase, respectively. The relaxation rate for each relaxation mechanism can be written in terms of spectral densities and, in Abragam's notation[31], takes the form

$$\frac{1}{T_1}(\omega_L,\Delta) = I(I+1)K_D\left[\sum_{m=0}^{2} f_{1m}(\Delta)\mathscr{J}^{(m)}(\omega_L) + \sum_{m=0}^{2} f_{2m}(\Delta)\mathscr{J}^{(m)}(2\omega_L)\right] \tag{14}$$

with $I = 1/2$ for proton NMR, $K_D = 3/2\left(\mu_0\gamma^2\hbar/(4\pi)\right)^2$. $\omega_L = 2\pi\nu_L = \gamma B$ is the Larmor frequency. Δ is the angle between the nematic director and the external magnetic field. In the case of the isotropic phase or mesophases with domains and an isotropic distribution of alignment directions - polycrystal, an integration of (14) on the solid angle 4π has to be made. Considering the functions $f_{kn}(\Delta)$ that can be found in[32] it is possible to obtain the averages

$$f_{kn}^{\mathrm{poly}} = \frac{1}{4\pi}\int_0^{2\pi}\int_0^{\pi} f_{kn}(\Delta) sin\Delta d\Delta d\phi = \frac{1}{5}\frac{b_k}{b_n}(2-\delta_{n0}) \tag{15}$$

with $b_k = 6,1,4$ for $k = 0,1,2$, respectively. δ_{ij} is the Kronecker delta.

In spite of the particular CB-C9-CB molecular structure with a slight bent shape, the molecule is still roughly rod-like with a length, ℓ, of about 30 Å and a width, d, of about 4.5 Å. In view of previous studies of molecular dynamics by proton NMR relaxation in liquid crystals BP8Cl-d17[33] and 9HL[34] we considered Nordio's model for the rotations/reorientations spin-lattice relaxation mechanism (R). Woessner model[35,36] is an alternative model used for different liquid crystals like 5CB[29]. The spin-lattice relaxation contribution is then given by the spectral densities $\mathscr{J}_R^{(k)}$[14,33]

$$\mathscr{J}_{\mathrm{R}}^{(k)}(\omega_L) = \frac{4}{3}b_k\sum_{m=0}^{2} A_m(\alpha_{ij},r_{ij})c(k,m)\frac{\tau_{k,m}^2}{1+\omega_L^2(\tau_{k,m}^2)^2} \tag{16}$$

with the correlation times $\tau_{k,m}^2$ given by

$$(\tau_{k,m}^2)^{-1} = D_z\left[\frac{1}{\beta_{k,m}^2} + \left(\frac{D_z}{D_x}-1\right)m^2\right] \tag{17}$$

$c(k,m)$ and $\beta_{k,m}^2$ can be estimated numerically as functions of the nematic order parameter S. $A_m(\alpha_{ij},r_{ij})$ factors are expressed in terms of the reduced Wigner matrices of second degree[14,29,33,34] where α_{ij} and r_{ij} are the inter-spin angles with the magnetic field and distances, respectively. $A_0 = \overline{|d_{0,0}^2(\alpha_{ij})|^2/r_{ij}^6} = \overline{(3\cos^2\alpha_{ij}-1)^2/(4r_{ij}^6)}$, $A_1 = 2\overline{|d_{1,0}^2(\alpha_{ij})|^2/r_{ij}^6} = \overline{3\sin^2 2\alpha_{ij}/(4r_{ij}^6)}$, $A_2 = 2\overline{|d_{2,0}^2(\alpha_{ij})|^2/r_{ij}^6} = \overline{3\sin^4\alpha_{ij}/(4r_{ij}^6)}$. $D_z \equiv \tau_{\parallel}^{-1}$ and $D_x \equiv \tau_{\perp}^{-1}$ are the rotational diffusion constants and corresponding correlations times, in the directions parallel and perpendicular to the molecular long axis, respectively.

In the limit case of zero order (isotropic phase) $\beta_{k,m}^2 = 1/6$ and $c(k,m) = 1/5$,[14,37] and the rotational diffusion constants will still reflect the effect of the molecular anisometry on the rotational motions

The values of A_m can be estimated from the CB-C9-CB molecules assuming an average molecular conformation using the molecular positions given by a molecular builder and visualization tool[38,39] (see table 1).

$\tau_{\parallel}$ and $\tau_{\perp}$ can be assumed to be thermally activated and dependent on the activations energies $E_{\parallel}$ and $E_{\perp}$, respectively, through Arrhenius expressions $\tau_{\parallel,\perp} = \tau_{\parallel,\perp}^{\mathrm{ref}}\exp[E_{\parallel,\perp}\mathscr{R}^{-1}(T^{-1} - T_{\mathrm{ref}}^{-1})]$, where $\tau_{\parallel,\perp}^{\mathrm{ref}}$ are the values of the correlation times for the reference temperature T_{ref} and $\mathscr{R}$ is the ideal gas-constant.

Translational self-diffusion is usually well described in the isotropic phase by the Torrey's model[40,41] that can be written in the form

$$\mathscr{J}_{\mathrm{SD}}^{(k)}(\omega_L) = \frac{n\tau_D}{d^3}j^{(k)}(\omega_L\tau_D,\alpha) \tag{18}$$

where $j^{(k)}(x)$ is dimensionless function found in[40], n is the density of spins and $\tau_D = \langle r^2\rangle/(6\mathscr{D})$ is the mean time between molecular jumps, $\mathscr{D}$ is the translational self-diffusion coefficient, d is the average distance between molecules, and $\alpha = \langle r^2\rangle/(12d^2)$.

In the nematic phase translational diffusion is better described by the model proposed by Žumer and Vilfan[42] where the spectral densities are not described by analytical expressions but obtained numerically. Generically, the spectral densities are like (18) except $j^{(k)}(x)$ becomes dependent on the nematic order parameter and on the distribution of spins along the molecule, and requires

two translational self-diffusion coefficients $D_\parallel$ and $D_\perp$ to account for the diffusion along the director and perpendicular to it, respectively.

$$\mathscr{J}^{(k)}_{\rm SDN}(\omega_L) = \frac{n\tau_{D_\perp}}{d^3} j^{(k)}_N\left(\omega_L\tau_{D_\perp}, \frac{\langle r^2\rangle}{d^2}, \frac{\ell}{d}, \frac{D^0_\parallel}{D^0_\perp}\right) \tag{19}$$

For a perfectly oriented nematic $D^0_\parallel/D^0_\perp = 2$ is found to be a reasonable approximation. $D_\perp = \mathscr{D}(1-S)+D^0_\perp S$ and $D_\parallel = \mathscr{D}(1-S)+D^0_\parallel S$, with $\mathscr{D} = (2D^0_\perp + D^0_\parallel)/3$. $\tau_{D_\perp} = \langle r^2\rangle/(4D^0_\perp)$.

Order director fluctuations observed in the nematic phases depend on the viscoelastic properties of the compounds. In the *one-constant approximation*: the K_1, twist, K_2, and bend, K_3 elastic constants are similar, $K_1 \sim K_2 \sim K_3 \sim K$, and the effective viscosity coefficients are also similar $\eta_1 \sim \eta_2 \sim \eta_3 \sim \eta$ and the spectral densities can be written as

$$\mathscr{J}^{(k)}_{\rm ODF}(\omega_L) = \delta_{k1} A_0 \frac{k_B T S^2}{\pi\sqrt{2}} \frac{1}{K}\sqrt{\frac{\eta}{K}} \frac{1}{\sqrt{\omega_L}}\left[g\left(\frac{\omega_{cM}}{\omega_L}\right) - g\left(\frac{\omega_{cm}}{\omega_L}\right)\right] \tag{20}$$

where k_B is the Boltzmman constant, $\omega_{cM} = 4\pi^2 K/(\eta\ell^2)$, $\omega_{cm} = 4\pi^2 K/(\eta\xi^2_\parallel)$ are the high and low cut-off frequencies, respectively. $\xi_\parallel$ is the coherence length of the fluctuation modes in the direction parallel to the director. $g(x)$ is given by

$$g(x) = \frac{1}{\pi}\left[\arctan\left(\sqrt{2x}-1\right) + \arctan\left(\sqrt{2x}+1\right) - arctanh\left(\frac{\sqrt{2x}}{x+1}\right)\right] \tag{21}$$

In a general situation the elastic constantes and effective viscosities are all different and (20) becomes more complex. Nevertheless, the dependence on the $\nu^{-1/2}$ is still observed. The prefactor $\sqrt{\eta/K^3}$ is replaced by $\sqrt{\eta_1/K_1^3}\sum_{m=1}^{2}\sqrt{K_1^3\eta_m/(\eta_1 K_m^2 K_3)}$. The cut-off functions become dependent on different cut-off frequencies defined in terms of the different elastic constants and viscosities, but the general effect on the relaxation dispersion is basically the same as that given by (21).

It was reported that the N_{tb} phase presents peculiar elastic properties that differentiate it from the classical nematic phase [26]. Therefore, the use of (20) can only be considered as a phenomenological first approximation that takes into account the observed Larmor frequency dependence $\sim \nu_L^{-1/2}$, and the existence of high and low cutoff frequencies. Probably, a specific model for this relaxation mechanism in the N_{tb} phase would present a different dependence of its amplitude on the viscoelastic parameters.

In the case of the isotropic phase it is possible to observe fluctuations of the order parameter as the result of on-set of nematic order in cybotactic clusters, when decreasing the temperature to the isotropic-nematic transition temperature. These small angle and short range nematic order oscillations, also known as order parameter oscillations, are described by spectral densities [14,29]

$$\mathscr{J}^{(k)}_{\rm OPF}(\omega_L) = \delta_{k1}\frac{1}{r^6_{\rm eff}}\frac{k_B T}{4\pi^2 K_{iso}}\sqrt{\frac{\eta_{\rm iso}}{K_{\rm iso}}} \frac{1}{\sqrt{\omega_L}}\int_0^{x_c}\frac{\sqrt{x}}{1+(x+\omega^{\rm iso}_{cm}/\omega_L)^2}dx \tag{22}$$

where $r_{\rm eff}$ is an average effective intermolecular spin distance, $x_c = \omega^{\rm iso}_{cM}/\omega_L$, $\omega^{\rm iso}_{cM} \sim K_{\rm iso}\pi^2/(\eta_{\rm iso}\ell^2)$ is the high cut-off frequency and $\omega^{\rm iso}_{cm} \sim K_{\rm iso}/(\eta_{\rm iso}\xi^2)$ depends on the coherence length associated with the size of nematic cybotactic domains in the isotropic phase and acts as a cut-off frequency in (22). It is worth to mention that numerically $(T_1^{-1})_{\rm OPF}$ and $(T_1^{-1})_{\rm ODF}$ can produce similar curves although with different model parameter values.

The model fitting to the experimental spin-lattice relaxation results considered a global least-squares minimisation procedure for all experimental results obtained in selected temperature ranges. The numerical least-squares minimisation was performed using *fitteia* [43].

Table 1 Model parameters obtained from the best fits of (13) to the experimental T_1^{-1} results in the isotropic, N, and N_{tb} phases of CB-C9-CB. $d \simeq 5\times10^{-10}$ m, $n \simeq 4.24\times10^{28}\,m^{-3}$. $D^{406K} \simeq 3.5\times10^{-11}\,m^2s^{-1}$, $E_D \simeq E_{D_\perp} \simeq 50\,kJmol^{-1}$. [28] $A_0 \simeq 5\times10^{57}\,m^{-6}$, $A_1 \simeq 2.7\times10^{57}\,m^{-6}$, $A_2 \simeq 7.6\times10^{57}\,m^{-6}$. The activation energies $E_\parallel \simeq 39\pm3$ kJmol^{-1}. $E_\perp \simeq 30\pm1$ kJmol^{-1} where obtained form the global fit.

Phase	Iso	N		N_{tb}		
T(K)	406	393	381	378	373	368
$\tau_\parallel$ (10^{-11}s)	7 ± 3	21 ± 1	31 ± 3	37 ± 2	40 ± 2	47 ± 2
$\tau_\perp$ (10^{-9}s)	2.3 ± 0.4	10 ± 1	8 ± 4	8.4 ± 0.5	9.4 ± 0.5	11 ± 1
τ_D (10^{-9}s)	1.2	3.4 ± 0.4	8.3 ± 0.8	9 ± 1	11 ± 1	14 ± 1
$A_{\rm OPF}$(10^4s$^{-3/2}$)	1.6 ± 0.4					
$\nu^{\rm iso}_{cm}$ (10^6Hz)	1.2 ± 0.5					
$\nu^{\rm iso}_{cM}$ (10^6Hz)	70 ± 10					
$A_{\rm ODF}$(10^3s$^{-3/2}$)		5.6 ± 0.6	14 ± 1	23 ± 2	33 ± 2	38 ± 2
ν_{cm} (10^4Hz)		2.3 ± 0.6	410 ± 30		820 ± 34	
ν_{cM} (10^6Hz)		>80	23 ± 2		26 ± 3	

3.2.3 Isotropic Phase

All experimental results obtained in the isotropic phase were analysed considering the model $T_1^{-1} = (T_1^{-1})_{\rm R} + (T_1^{-1})_{\rm SD} + (T_1^{-1})_{\rm OPF}$ and the fitting parameters were D, $\tau_\parallel$, $\tau_\perp$, $\nu^{\rm iso}_{cm}$, $\nu^{\rm iso}_{cM}$, and the strength of the OPF contribution, $A_{\rm OPF} = 3K_D k_B T\sqrt{\eta_{\rm iso}}/(16 r^6_{\rm eff}\pi^2 K^{3/2}_{iso})$, obtained from (14) and (22). In view of the fact that both frequency and temperature dependences are taking into account simultaneously in the fitting process, it was necessary to consider the activation energies $E_{\rm D}$, $E_\parallel$, and $E_\perp$, for the SD, and R correlation times, respectively and, in addition, linear temperature dependences were assumed for both $A_{\rm OPF}$ and $\nu^{\rm iso}_{cm}$. $A_{\rm OPF} = 2\times10^4 - 5\times10^2(T-T_{\rm NI})$ for $T < 404$K, otherwise $A_{\rm OPF} \simeq 0$. $\nu^{\rm iso}_{cm} = 1.5\times10^5 + 1.2\times10^5(T-T_{\rm NI})$ for $T > T_{NI}$. In the case of $(T_1^{-1})_{\rm SD}$, values of $\mathscr{D}$ close to those obtained for CB-C7-CB [28] were considered (see table 1).

The best fitting curves to the experimental results, obtained with fitting model (13), are presented in figure 10 . The translational self-diffusion contribution is basically fixed due to the fact that the translational self-diffusion coefficient of CB-C9-CB is not

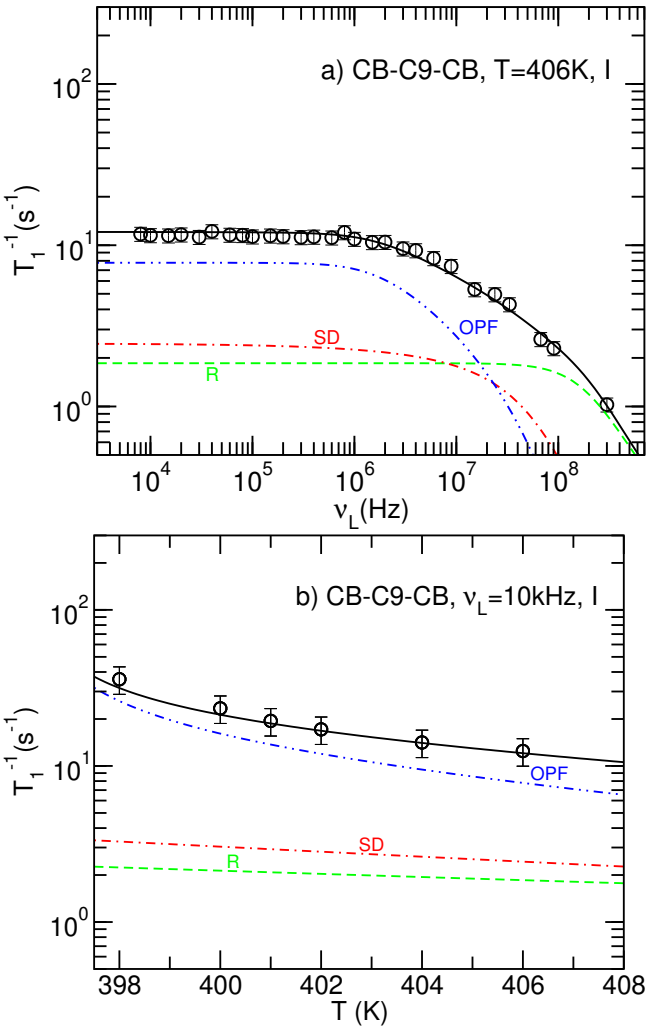

Fig. 10 (Color online) Best model fits to the CB-C9-CB experimental spin-lattice relaxation results in the isotropic phase, using (13), (14), (16), (18), and (22) as explained in the text. a) T_1^{-1} dispersion at T=406 K; b) T_1^{-1} as a function of temperature, for $\nu_L = 10$ kHz. The T_1^{-1} curves corresponding to the relaxation contributions are also presented.

expected to be that much different from that of CB-C7-CB. Actually, $D_{5CB} \simeq 5.4 \times 10^{-11} m^2 s^{-1}$ at 313K (4 degrees above T_{NI}^{5CB}), a value close to the values measured for CB-C7-CB four degrees above T_{NI}[28]. The activation energies E_D for the two compounds are also not very different[28,29,44].

The T_1^{-1} dispersion and temperature dependence fits show that rotations and order parameters fluctuations are the most relevant relaxation mechanisms above 50 MHz and below 10 MHz, respectively. The activation energies $E_{\|}$ and $E_{\perp}$ could not be determined precisely and values close to those obtained for 5CB were used[29].

From the ratio $\omega_{cM}^{iso}/\omega_{cm}^{iso}$ it is possible to estimate the ratio ξ/ℓ that gives one idea about the relative size of the cybotactic clusters in the isotropic phase. This ratio presents a strong temperature dependence close to T_{NI}, for $T \geq T_{NI}$, decreasing from about 20 to 8 molecular lengths as the temperature decreases from T_{NI}. The values $K_{iso} \sim 3 \times 10^{-12}$ N and $\eta_{iso} \sim 0.02$ Pa.s could be estimated from the A_{OPF} and ω_c^{iso} cut-off frequencies. These values are close to those obtained for 5CB liquid crystal[45,46]

3.2.4 High Temperature Nematic Phase, N

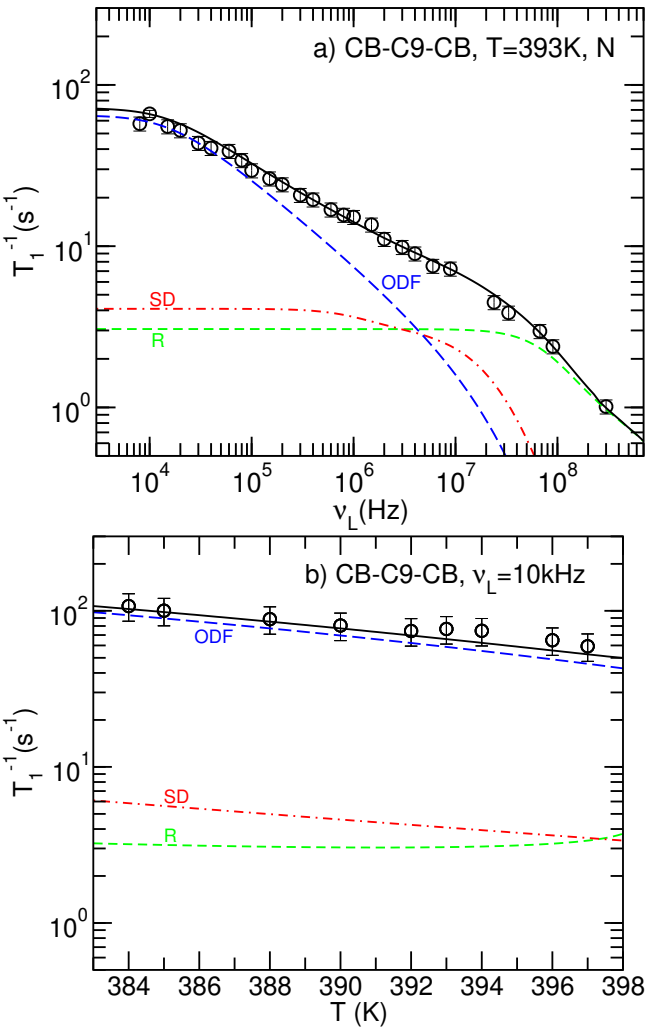

Fig. 11 (Color online) Best model fits to the CB-C9-CB experimental spin-lattice relaxation dispersion results obtained at $T = 393$ K and T_1^{-1} in the temperature range 384K – 397K for a few selected frequencies, using (13), (14), (16), (19), and (20) as explained in the text. a) T_1^{-1} dispersion at T=393 K; b) T_1^{-1} as a function of temperature, for $\nu_L = 10$ kHz. The T_1^{-1} curves corresponding to the relaxation contributions are also presented.

The experimental data and model fitting curves, corresponding to the best model fit of (13), considering the global minimisation of the least-squares for all experimental results, are presented in figure 11 . As it was verified that the director alignment depended on the value of the applied magnetic field and a good alignment was observed only for fields above 0.2 T an isotropic distribution of domains was assumed for the spectral densities (14), which were calculated using (15). The fitting parameters obtained for these fits are presented in table 1. The prefactor of the ODF contribution, $A_{ODF} = 3K_D A_0 k_B T S^2 \sqrt{\eta}/(4\pi\sqrt{2}K^{3/2})$, obtained from (14) and (20), and the low cut-off frequency of the ODF relaxation contribution were assumed to be temperature dependent: $A_{ODF} = 7.6 \times 10^3 - 2.3 \times 10^2 (T - 406)$, $\nu_{cm} = 1.8 \times 10^6 (1 - T/353)^2$.

The temperature dependence of the order parameter considered was $S = (1 - T/398.5)^{0.13}$, according to expression (9) with the corresponding fitting parameters referred in section 3.1 . The temperature dependence of ν_{cM} could not be estimated from the data analysis. The fitting parameters are presented in table 1. The translational self-diffusion coefficient was assumed to be close to that obtained for CB-C7-CB[28].

3.2.5 Low Temperature Nematic Phase, N_{tb}

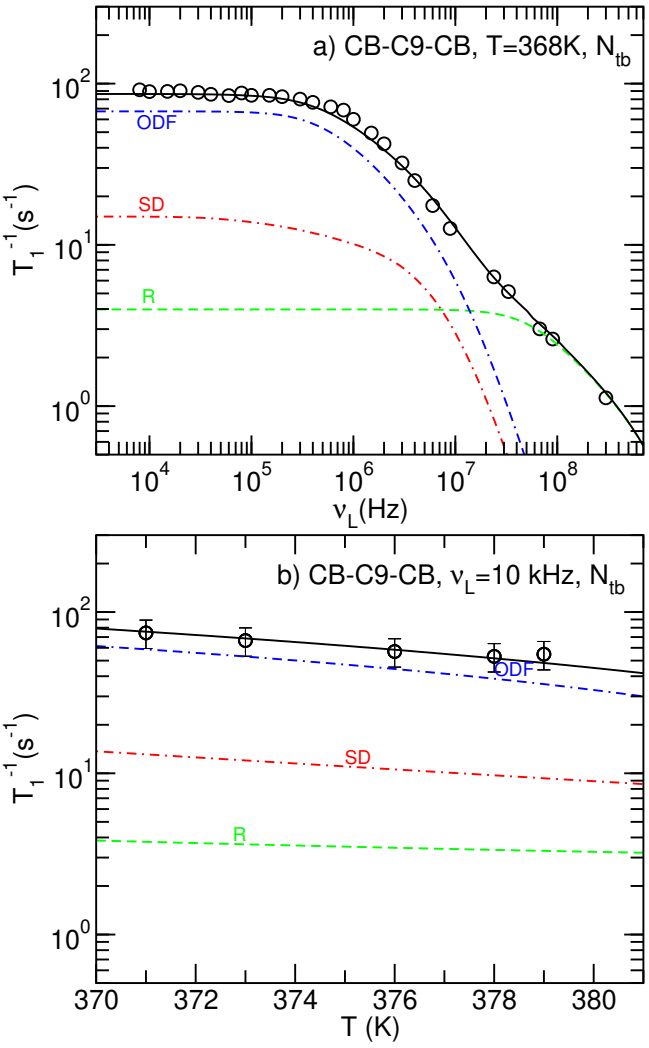

Fig. 12 (Color online) a) Best model fits to the CB-C9-CB experimental spin-lattice relaxation dispersion results obtained at $T = 368$ K, using (13), (14), (16), (19), and (20) as explained in the text. The T_1^{-1} curves corresponding to the relaxation contributions are also presented. b) T_1^{-1} as a function of temperature, for $\nu_L = 10$ kHzin the N_{tb} phase. The T_1^{-1} curves corresponding to the relaxation contributions are also presented.

The experimental data and model fitting curves, corresponding to the best fit considering the global minimisation of the least-squares for all experimental results, are presented in figure 12 . The temperature fits are similar to those obtained for the other mesophase (N). The fitting parameters obtained from these fits are presented in table 1. The prefactor and the low cut-off frequency of the ODF relaxation contribution were assumed to be temperature dependent: $A_{ODF} = 1.8 \times 10^4 - 1.6 \times 10^3 (T - 406)$, $\nu_{cm} = 8.7 \times 10^5 (1 - T/4000)^2$. The temperature dependence of ν_{cM} could not be estimated from the data analysis. The fitting parameters are presented in table 1. The translational self-diffusion coefficient was assumed to be close to that obtained for CB-C7-CB[28].

3.2.6 Global analysis of proton NMR Relaxation

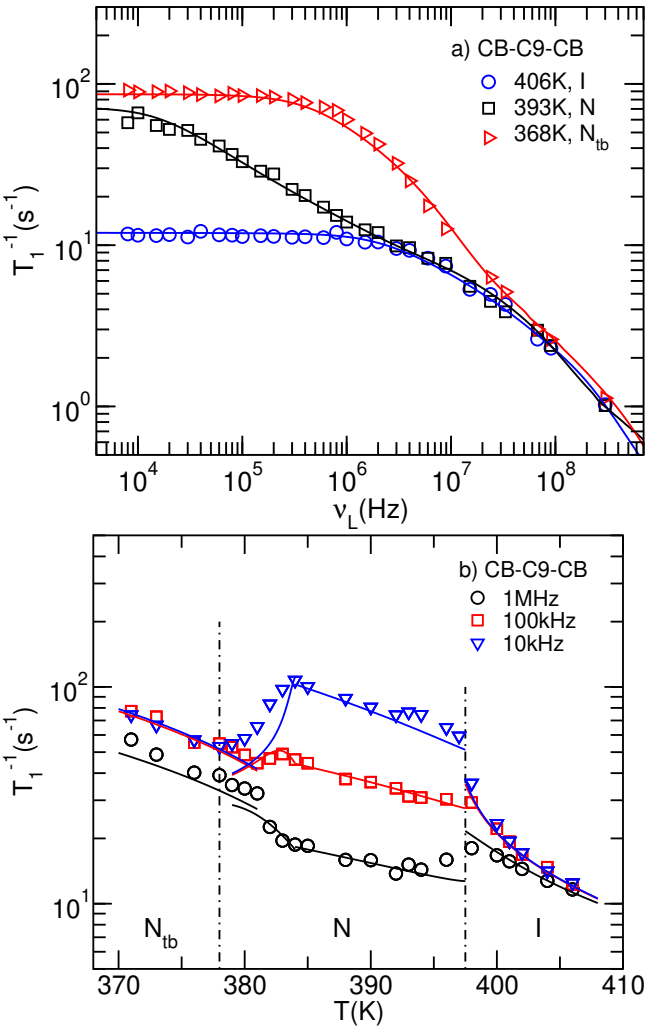

Fig. 13 (Color online) Experimental data and T_1^{-1} fitting curves obtained for CB-C9-CB, using (13), as explained in the text. a) T_1^{-1} as a function of frequency for three selected temperatures in the isotropic, N, and N_{tb} phases. b) T_1^{-1} as a function of temperature for for three selected frequencies.

The global analysis of the proton spin-lattice relaxation shows that the main features of the relaxation dispersion and temperature dependences could be well explained by the relaxation model considered. The major discrepancy can be seen on the model fit of the temperature dependence for temperatures between 383K and 379K. This issue was found to be related to different cooling processes associated with the measurements of T_1^{-1} as a function of frequency and temperature in the different NMR experimental setups used. For the T_1^{-1} vs ν_L measurements the sample remained at the desired temperature during a much longer period of time

after a cooling process from the isotropic phase at a fixed cooling rate, where as for the temperature measurements the sample remains at one temperature just the time necessary to perform the measurement of T_1^{-1} a few times, thus a much shorter time.

The fitting parameters are presented as a function of temperature in figure 15 . The ratio ξ/ℓ was obtained from the ratio between the high and low cut-off frequencies obtained for the collective motions relaxation contribution. This ratio gives an estimation of the linear dimensions of a molecular cluster or cybotactic domain (in the case of the isotropic phase) and it varies from 8 molecular lengths in the isotropic phase to 80 molecular lengths in the nematic phase. This value decreases significantly with decreasing temperature at the N-N_{tb} phase transition to values close to those of the isotropic phase for a N_{tb} non-aligned system. The strength of the CM contribution varies with temperature and presents different behaviours in different phases. It is worth mention that in the isotropic phase the OPF contribution as detected at 10 kHz in figure 13b presents a strong increase close to T_{NI} and has associated to it a strong increase of $\xi_{\|}/\ell$ as is observed in figure 15b.

In the nematic phase both A_{ODF} and $\xi_{\|}/\ell$ present monotonous increase with decreasing temperature. It is interesting to note that, when using reported values of the visco-elastic constantes measured for CB-C9-CB liquid crystals[26] to estimate A_{ODF}, using (20), the values overlap very well with those obtained from the analysis of T_1^{-1} data, thus supporting the proposed relaxation model. Below, 384K it is clear that the molecular organization changes and a abrupt decrease of $\xi_{\|}/\ell$ is observed and A_{OPF} presents a steeper increase with decreasing temperature. The molecular reorganization process perceived by an increase of the low cut-off frequency (see insert plot in figure 15b) is clear associated with a breaking of director fluctuations with long wave lengths, with is compatible with a non-uniform director field like that proposed for the twist-bend director field. The change observed in the director field before the reported N-N_{tb} phase transition temperature seems to stabilise for temperatures below 380K according to the behaviour of $\xi_{\|}/\ell$. The A_{ODF} continues to increase with decreasing temperature due to the change in the visco-elastic constants with temperature.

The relaxation model considered to interpret the spin-lattice relaxation results in the N_{tb} phase included the same three relaxation mechanisms considered for the N_u phase. In this approximation the specfic twist–bend molecular organization on the phase was not directly incorporated in the model except for the fact that a uniform distrubution of domain orientations was considered when calculating T_1^{-1}. In fact in view of the helical distribution of molecular orientations in the domains in the N_{tb} it is possible that *rotations induced by diffusion* (RiD) become also an effective relaxation mechanism. To now no specific relaxation model has been proposed to account for the relaxation contribution associated with this specific relaxation contribution in the N_{tb} phase. Nevertheless, at first approximation it possible to consider the model proposed for the relaxation mechanism associated to the diffusion induced rotation of molecules along the helical axis in cholesteric phases[47]. In this case

$$(T_1^{-1})_{RiD} = I(I+1)K_D 2\frac{\tau_{RiD}}{r_e^6}\left(\frac{f_{12}^{poly}}{1+\omega_L^2\tau_{RiD}^2}+\frac{f_{22}^{poly}}{1+4\omega_L^2\tau_{RiD}^2}\right), \quad (23)$$

with $\tau_{RiD} = p^2/(16\pi^2 D_h)$, where p is the helical pitch and D_h is the diffusion component along the helical axis. The value of the pitch is not known for CBC9CB. However, in view of the pitch values range $79-100$ Å reported for a similar CBC7CB, assuming $p \sim 85$ Å and $D_h \sim D_{||} \sim 2D_{\perp}$, and an average intramolecular spin-pair distance $r_e \sim 3.3$ Å the contribution $(T_1^{-1})_{RiD}$ can be estimated and its effect on the model fit of T_1^{-1} dispersion at 368K can be seen in fig. 14.

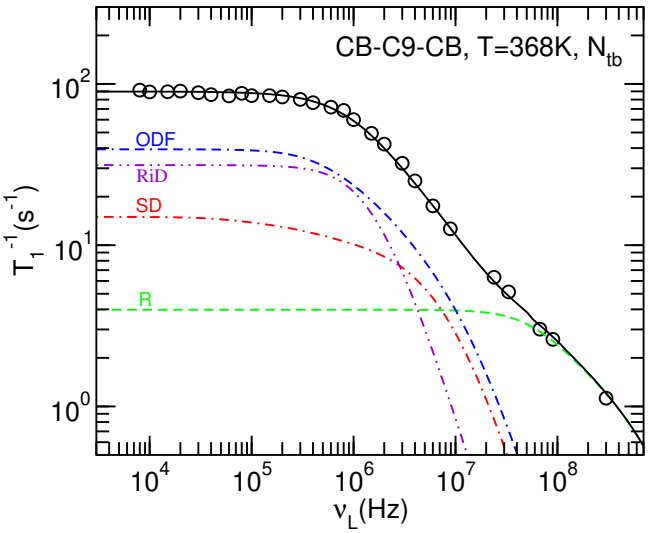

Fig. 14 (Color online) Model fitting of T_1^{-1} dispersion in the N_{tb} phase at $T = 368$ K, using $T_1^{-1} = (T_1^{-1})_R + (T_1^{-1})_{SD} + (T_1^{-1})_{ODF} + (T_1^{-1})_{RiD}$ with (14), (16), (19), (20), and (23), as explained in the text. The contributions of SD and R are the same as those of 12(a). The ODF contribution changed to compensate the inclusion of RiD contribution.

As it can be seen in fig. 14 the fit is as good as that of fig. 12(a). In fact both contributions are relevant in the same frequency region and are, therefore, difficult to decouple. Still, it is important to note that the complete replacement of ODF by RiD would produced clear worst model fits. The amplitude of ODF, $A_{odf} \sim 22\times10^3 s^{-3/2}$, decreases as the result of the additional RiD relaxation contribution.

3.3 Proton spectroscopy and relaxometry discussion

This approach puts together information on molecular order and dynamics giving an insight on the influence of the phases' structure on the molecular motions. Both the spectroscopy and relaxometry data show very clear differences between the N and the N_{tb} phases.

The results obtained by these two NMR experimental techniques in the N phase are in line with conclusions previously reported on 5CB and other typical nematic phases[29]. In addition, the similarity of proton NMR relaxation results in the isotropic phase of CBC9CB and 5CB makes it possible to conclude that the

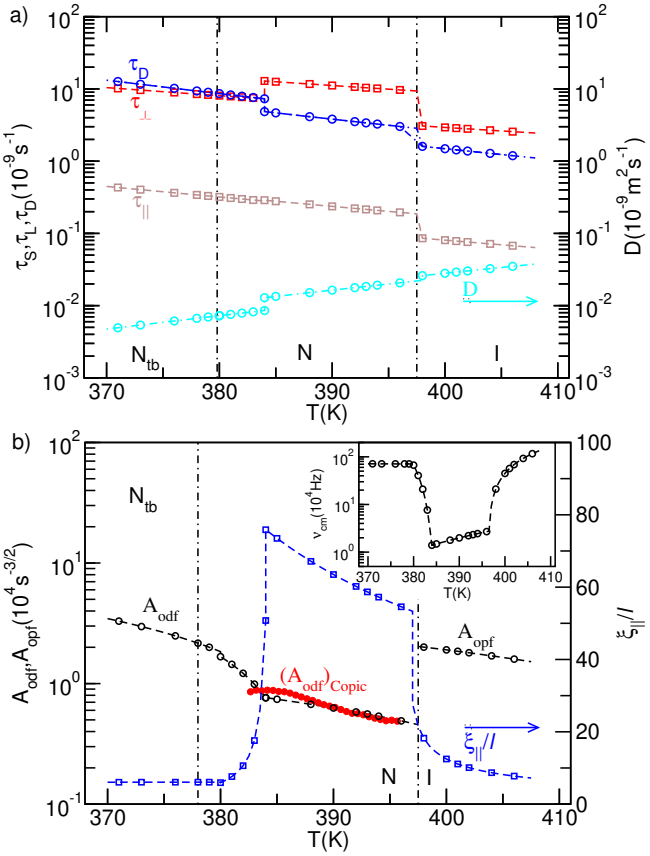

Fig. 15 (Color online) Model fitting parameters as a function of temperature, corresponding to the best fits. In filled red circles are presented the estimated values of A_{ODF} calculated with the expression fo the ODF prefactor of (20) considering distinct elastic constants and viscosities $\sqrt{\eta_1/K_1^3}\sum_{m=1}^{2}\sqrt{K_1^3\eta_m/(\eta_1 K_m^2 K_3)}$ and the values for the visco-elastic constants reported by Čopič[26].

individual role of monomers is crucial to the behavior of these two phases. On the other hand, regarding the lower temperature N_{tb} phase, the correlation between the biphenyl mesogenic cores of a dimer is essential to the formation of a more complex local molecular arrangement characteristic of that phase.

With respect to spectroscopy data, high field ($B_0 = 7$T, $\nu_L =$ 300MHz) and low field ($B_0 = 0.78$T, $\nu_L = 33.4$MHz) results show a noticeable distinction between the N and the N_{tb} phases.

In the case of high field data, the proton dipolar splitting increases with decreasing temperature in the N phase, as expected due to the corresponding increasing of the nematic order parameter S as the molecular alignment is enhanced. The evolution of S with the temperature is consistent with the Haller law[25]. However, on crossing the N-N_{tb} phase transition, starting 4-5 °K above, the splitting decreases with decreasing temperature. This difference is explained by the onset of some tilting of the molecular axis with respect to the nematic director. The data are compatible with an increasing of this tilting and an increasing twisting of the aliphatic groups with decreasing temperature. This result is consistent with descriptions of the N_{tb} phase presented in the literature, namely with the decreasing of the helical pitch with decreasing temperature in the N_{tb} phase observed in similar systems by means of resonant X-ray scattering[12,13].

Low field data are noticeably different for the N and the N_{tb} phases. In the N phase, the spectra are of the same type of those observed for high field, with a pair of broad peaks characteristic of the dipolar splitting resulting from an aligned monodomain. For lower temperatures corresponding to the N_{tb} phase, the spectra changes significantly, revealing a partial orientation of the sample. This effect shows that, in contrast to the process in the N phase, the magnetic torque necessary for the common alignment of the nematic director in the N_{tb} is higher than can be reached with the $B_0 = 0.78$T field.

Regarding the relaxometry results, the most noticeable feature of the T_1^{-1} dispersion data is the unusual low frequency plateau in the N_{tb} phase when compared with other nematic systems. Beyond this, the N-N_{tb} phase transition is clearly observable in the plots of T_1^{-1} as a function of temperature (see Figures 9 and 13). These noticeable features indicate that the molecular organization of the N_{tb} phase is strongly conditioning the molecular dynamics, particularly on the low Larmor frequency domain, normally dominated by the slow collective motions.

From the global analysis of the data obtained in the three phases studied (I, N and N_{tb}) it is possible to conclude that the variations with temperature of the correlation times associated to local molecular rotations/reorientations and of the average time between diffusive jumps (and consequently the diffusion coefficients) are compatible with Arrhenius expressions characteristic of thermally activated mechanisms (see Figure 15 a)).

The rotational diffusion coefficients, the corresponding correlation times, and the magnitude of the corresponding activation energies, in the studied phases, are in line with typical values for other low molecular weight liquid crystals with molecules with ℓ/d of the same order of magnitude[29,33,48].

The relaxation contributions considered for the self-diffusion mechanism in the isotropic phase and in the N and N_{tb} phases are overall in accord with the values of diffusion coefficient and activation energy reported for 5CB and for the compound CB-C7-CB using direct diffusion measurements by PFG ^{1}H NMR method[28].

From the maximum and minimum cutoff frequencies associated to the OPF or ODF mechanisms it was possible to obtain an estimate of the ratio $\xi_{\parallel}/\ell$ that is related to the relative size of the nematic domains or cybotactic clusters in the case of the isotropic phase. From figure 15 b), it is possible to observe that this ratio shows a steep increase with decreasing temperature at the transition between the isotropic phase and the classical nematic (N) phase (changing from about 8 to close to 80 molecular lengths). This is expected as the number of molecules in a nematic domain is obviously much higher than that observed for the cybotactic clusters in the isotropic phase. Surprisingly, accordingly to the fits, this ratio decreases again with decreasing temperature at the transition between the N and N_{tb} phases, indicating a short correlation length for collective nematic order director fluctuations in the N_{tb} phase (in the non-aligned N_{tb} phase the clusters have a linear dimension of about 8 molecular lengths). This may may be an indication of hierarchical self assembly structures found for these systems.[49]

The parameters of K_{iso} and η_{iso} estimated for CB-C9-CB from A_{OPF} and ω_c^{iso} are also in line with the values reported for the liquid crystal 5CB[45,46].

The consistence of the results obtained both as a function of the Larmor frequency and temperature (see figures 13 and 15), is reinforced by the overall agreement between the fitting parameters obtained and values corresponding to the results of alternative measurements by complementary experimental techniques reported elsewhere[26,28,45,46]. It is particularly noticeable that the values of the ODF mechanism prefactor A_{ODF}, as a function of temperature estimated using (20) and the values of the viscoelastic constantes measured for CB-C9-CB liquid crystals[26], very closely agree with those obtained from the analysis of the proton relaxation data obtained in this study, as shown in figure 15.

Besides the very clear distinction between the classical nematic phase and the N_{tb} phase, it is worthwhile to stress the consistence between the results obtained from NMR spectroscopy and relaxometry. The results of NMR spectroscopy, show that, for low static NMR field, a partial orientation distribution of the nematic director exists in the N_{tb} phase with the local director tilted with respect to the N_{tb} global director in a nematic domain. These results agree with the relaxation data (in particular those associated with the ODF mechanism) indicating the presence of molecular domains much smaller in the N_{tb} phase than in the conventional N phase.

4 Conclusions

The work presented herein is, to our knowledge, the first study combining proton NMR spectroscopy and relaxometry in the nematic phases of the CBC9CB dimer with particular attention to the peculiar N_{tb} phase. Very clear differences between the N phase and the N_{tb} phase are observed both by proton NMR spectroscopy and relaxometry. Spectroscopy analysis at high magnetic fields has detected an increasing molecular tilt in the N_{tb} as temperature decreases. This result is in agreement with the proposed structure for this phase, in particular the decreasing of the helical pitch with decreasing temperature in the N_{tb} phase, as reported in the literature on the basis of resonant X-ray scattering measurements. At low magnetic fields, spectroscopy analysis has detected a polydomain N_{tb} phase sample, in accord with the rope director structure observed by POM in this phase. Relaxometry results in the isotropic and nematic phases of CBC9CB are similar to those obtained in 5CB, reinforcing the central role that the individual monomers play in these phases. In all phases studied, relaxometry analysis showed that local molecular rotations reorientations and translational self diffusion processes are thermally activated processes with correlation times and diffusion constants following Arrhenius type laws. Significant pre-transitional effects were observed at the N-N_{tb} phase transition both from relaxometry and spectroscopy data. In the N_{tb} phase, the relaxometry results show an unusual plateau in the spin lattice relaxation rate dispersion which is identified with a significant decrease of the correlation length for the collective modes in comparison with the N phase. This result is compatible with the non-uniform local director field characteristic of the N_{tb} phase, associated with a helical structure with a pitch of the order of magnitude of the estimated correlation length for the collective modes.

Conflicts of interest

There are no conflicts to declare.

Acknowledgements

The authors acknowledge financial support from: - Portuguese Science and Technology Foundation (FCT) through CeFEMA strategic project UID/CTM/04540/2013; - European Union through Grant FP7-PEOPLE-2007-1-1-ITN-215884 (DENDREAMERS); - European Union and the Portuguese Science and Technology Foundation (FCT) through Grant M-ERA-NET2/0006/2016 (CellColor)

References

1 L. M. Blinov and V. G. Chigrinov, *Electrooptic Effects in Liquid Crystal Materials*, Springer New York, 1994.

2 V. P. Panov, M. Nagaraj, J. K. Vij, Y. P. Panarin, A. Kohlmeier, M. G. Tamba, R. A. Lewis and G. H. Mehl, *Physical Review Letters*, 2010, **105**, 167801.

3 C. S. P. Tripathi, P. Losada-Perez, C. Glorieux, A. Kohlmeier, M.-G. Tamba, G. H. Mehl and J. Leys, *Physical Review E*, 2011, **84**, 041707.

4 M. Cestari, S. Diez-Berart, D. A. Dunmur, A. Ferrarini, M. R. de la Fuente, D. J. B. Jackson, D. O. Lopez, G. R. Luckhurst, M. A. Perez-Jubindo, R. M. Richardson, J. Salud, B. A. Timimi and H. Zimmermann, *Physical review. E, Statistical, nonlinear, and soft matter physics*, 2011, **84**, 031704.

5 V. Borshch, Y. K. Kim, J. Xiang, M. Gao, A. Jakli, V. P. Panov, J. K. Vij, C. T. Imrie, M. G. Tamba, G. H. Mehl and O. D. Lavrentovich, *Nature Communications*, 2013, **4**, 2635.

6 I. Dozov, *Europhysics Letters*, 2001, **56**, 247–253.

7 K. Hori, M. Iimuro, A. Nakao and H. Toriumi, *Journal of Molecular Structure*, 2004, **699**, 23–29.

8 K. Krzyzewska, T. Jaroch, A. Maranda-Niedbala, D. Pociecha, E. Gorecka, Z. Ahmed, C. Welch, G. H. Mehl, A. Pron and R. Nowakowski, *Nanoscale*, 2018, **10**, 16201–16210.

9 J. S. Patel and R. B. Meyer, *Physical Review Letters*, 1987, **58**, 1538–1540.

10 K. L. Atkinson, S. M. Morris, F. Castles, M. M. Qasim, D. J. Gardiner and H. J. Coles, *Physical Review E*, 2012, **85**, 012701.

11 A. Hoffmann, A. G. Vanakaras, A. Kohlmeier, G. H. Mehl and D. J. Photinos, *Soft Matter*, 2015, **11**, 850–855.

12 C. H. Zhu, M. R. Tuchband, A. Young, M. Shuai, A. Scarbrough, D. M. Walba, J. E. Maclennan, C. Wang, A. Hexemer and N. A. Clark, *Physical Review Letters*, 2016, **116**, 147803.

13 W. D. Stevenson, Z. Ahmed, X. B. Zeng, C. Welch, G. Ungar and G. H. Mehl, *Physical Chemistry Chemical Physics*, 2017, **19**, 13449–13454.

14 R. Dong, *Nuclear magnetic resonance of liquid crystals*, Springer New York, 1997.

15 F. Noack, *Progress In Nuclear Magnetic Resonance Spectroscopy*, 1986, **18**, 171–276.

16 B. Robles-Hernández, N. Sebastián, M. R. de la Fuente, D. O. López, S. Diez-Berart, J. Salud, M. B. Ros, D. A. Dunmur,

G. R. Luckhurst and B. A. Timimi, *Physical Review E*, 2015, **92**, 062505.
17 L. Beguin, J. W. Emsley, M. Lelli, A. Lesage, G. R. Luckhurst, B. A. Timimi and H. Zimmermann, *Journal of Physical Chemistry B*, 2012, **116**, 10407–10407.
18 J. Emsley, M. Lelli, A. Lesage and G. R. Luckhurst, *J. Phys. Chem. B*, 2013, **117**, 6547:6557.
19 R. Dong, A. Kohlmeier, M. Tamba, G. Mehl and E. Burnell, *Chemical Physics Letters*, 2012, **552**, 44:48.
20 B. R. Hernandez, N. Sebastian, M. R. de la Fuente, D. O. Lopez, S. D. Berart, J. Salud, D. A. Ros, M. Blanca ans Dunmur, G. R. Luckhurst and B. A. Timimi, *PHYSICAL REVIEW E*, 2015, **92**, 062505:1:16.
21 E. E. Burnell, Z. Ahmed, C. Welch, G. H. Mehl and R. Y. Dong, *Chemical Physics Letters*, 2016, **659**, 48–54.
22 J. W. Emsley, M. Lelli, H. Joy, M. G. Tamba and G. H. Mehl, *Physical Chemistry Chemical Physics*, 2016, **18**, 9419–9430.
23 C. Greco, G. R. Luckhurstb and A. Ferrarini, *Phys.Chem. Chem. Phys.*, 2013, **15**, 14961,14965.
24 S. M. Salili, M. G. Tamba, S. N. Sprunt, C. Welch, G. H. Mehl, A. Jakli and J. T. Gleeson, *Physical Review Letters*, 2016, **116**, 217801.
25 I. Haller, *Progress in Solid State Chemistry*, 1975, **10, Part 2**, 103:108.
26 A. Mertelj, M. Čopič, G. R. Luckhurst, R. P. Tuffin and O. Parri, 12th European Conference on Liquid Crystals, ECLC-2013, 2013.
27 K. Adlem, M. Copic, G. R. Luckhurst, A. Mertelj, O. Parri, R. M. Richardson, B. D. Snow, B. A. Timimi, R. P. Tuffin and D. Wilkes, *Physical Review E*, 2013, **88**, 022503.
28 M. Cifelli, V. Domenici, S. Dvinskikh, G. Luckhurst and B. Timimi, *Liquid Crystals*, 2017, **44**, 204–218.
29 P. J. Sebastião, A. Gradišek, L. F. V. Pinto, T. Apih, M. H. Godinho and M. Vilfan, *Journal of Physical Chemistry B*, 2011, **115**, 14348–14358.
30 A. Aluculesei, F. Vaca Chávez, C. Cruz, P. J. Sebastião, N. G. Nagaveni, V. Prasad and R. Y. Dong, *The journal of physical chemistry. B*, 2012, **116**, 9556–63.
31 A. Abragam, *The Principles of Nuclear Magnetism*, Clarendon Press, Oxford, 1961.
32 P. Ukleja, J. Pirs and J. W. Doane, *Phys. Rev. A*, 1976, **14**, 414–423.
33 A. Ferraz, J. Zhang, P. J. Sebastião, A. C. Ribeiro and R. Y. Dong, *Magnetic Resonance In Chemistry*, 2014, **52**, 546–555.
34 A. Gradišek, V. Domenici, T. Apih, V. Novotnáa and P. J. Sebastião, *J. Phys. Chem. B*, 2016, **120**, 4706–4714.
35 D. E. Woessner, *The Journal of Chemical Physics*, 1962, **36**, 1–4.
36 D. E. Woessner, *The Journal of Chemical Physics*, 1962, **37**, 647–654.
37 C. R. Cruz, J. L. Figueirinhas and P. J. Sebastião, *NMR of Liquid Crystal Dendrimers*, Pan Stanford Publishing Pte. Ltd., Singapore, 2017.
38 Avogadro: an open-source molecular builder and visualization tool. Version 1.2.0 http://avogadro.cc/.
39 M. D. Hanwell, D. E. Curtis, D. C. Lonie, T. Vandermeersch, E. Zurek and G. R. Hutchison, *Journal of Cheminformatics*, 2012, **4**, 17.
40 H. C. Torrey, *Physical Review*, 1953, **92**, 962–969.
41 J. F. Harmon and B. H. Muller, *Phys. Rev.*, 1969, **182**, 400–410.
42 S. Žumer and M. Vilfan, *Physical Review A*, 1978, **17**, 424–433.
43 P. J. Sebastião, *European Journal of Physics*, 2014, **35**, 015017.
44 S. V. Dvinskikh, I. Furó, H. Zimmermann and A. Maliniak, *Phys. Rev. E*, 2002, **65**, 061701.
45 A. G. Chmielewski and E. Lepakiewicz, *Rheologica Acta*, 1984, **23**, 207–210.
46 J. D. Bunning, T. E. Faber and P. L. Sherrell, *Journal De Physique*, 1981, **42**, 1175–1182.
47 M. Vilfan, R. Blinc, J. Dolinšek, M. Ipavec, G. Lahajnar and S. Žumer, *Journal de Physique*, 1983, **44**, 1179–1184.
48 A. Gradišek, V. Domenici, T. Apih, V. Novotnáa and P. J. Sebastião, *J. Phys. Chem. B*, 2016, **120**, 4706–4714.
49 V. P. Panov, S. P. Sreenilayam, Y. P. Panarin, J. K. Vij, C. J. Welch and G. H. Mehl, *Nano Letters*, 2017, **17**, 7515–7519.

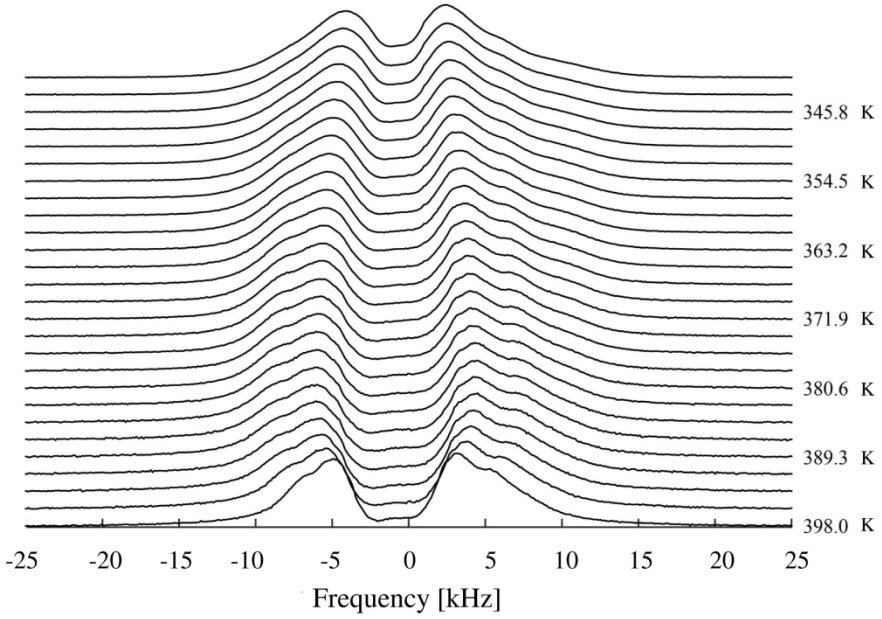

254x190mm (300 x 300 DPI)

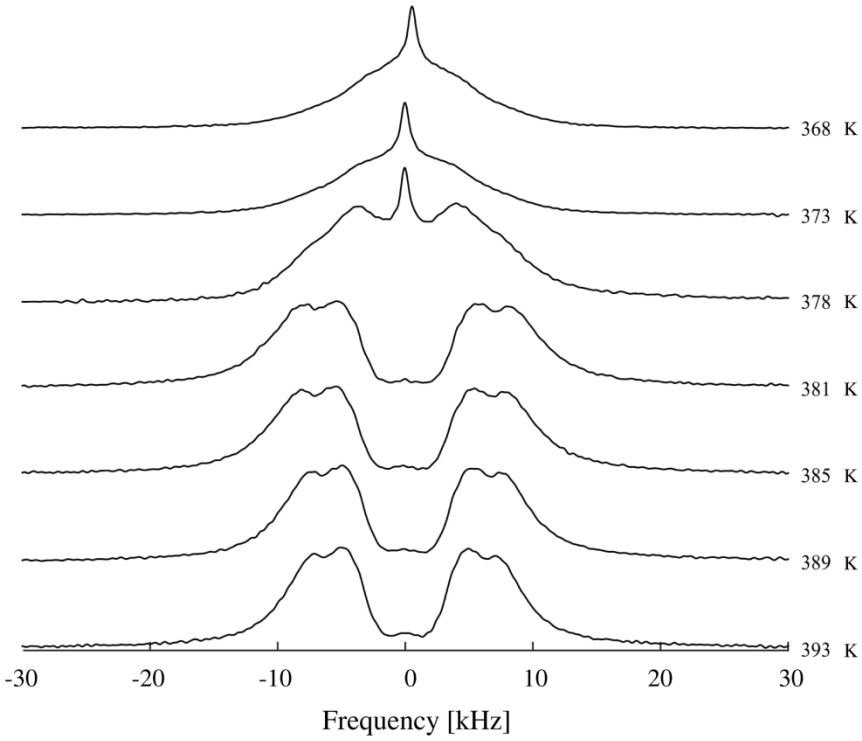

254x190mm (300 x 300 DPI)

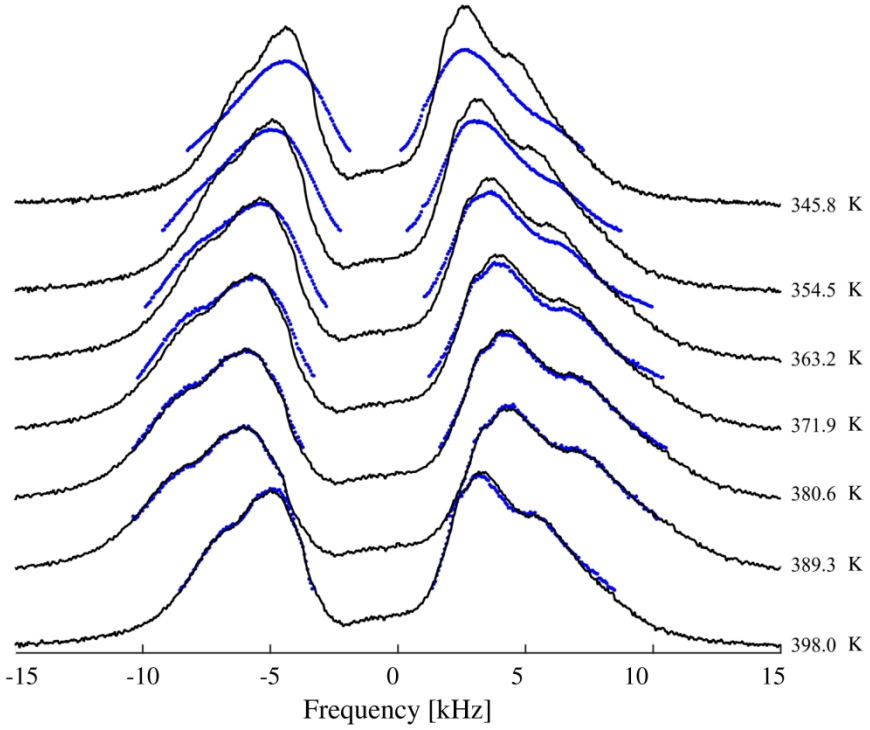

254x190mm (300 x 300 DPI)

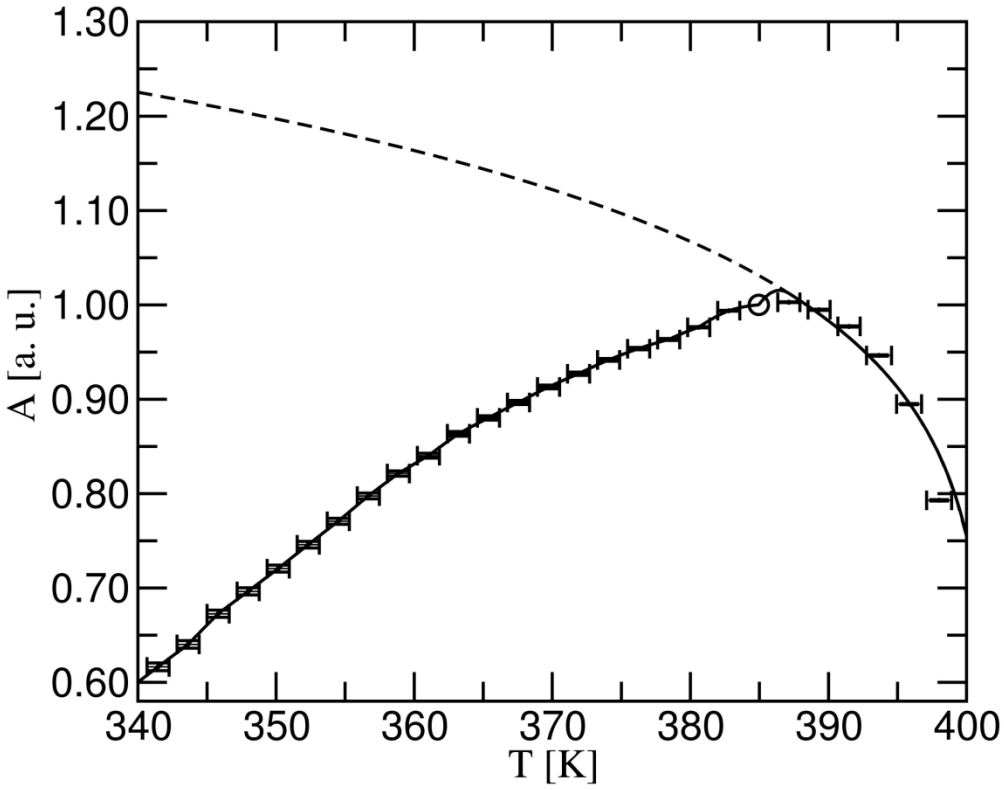

217x170mm (300 x 300 DPI)

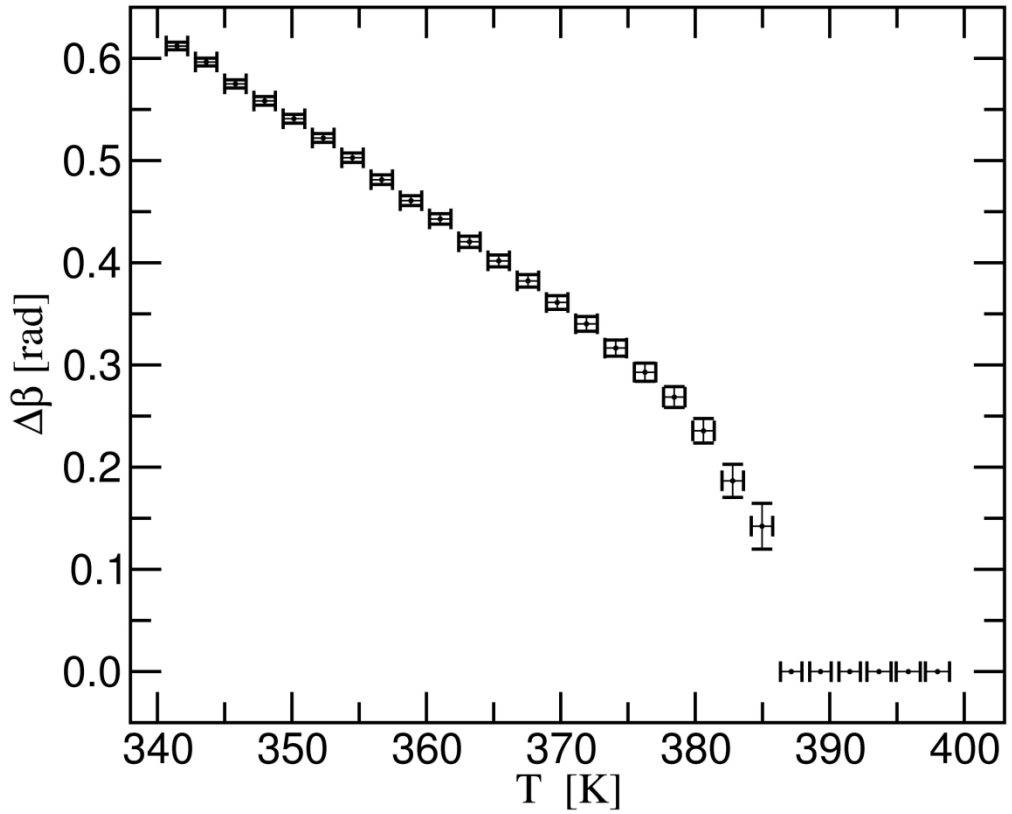

207x167mm (300 x 300 DPI)

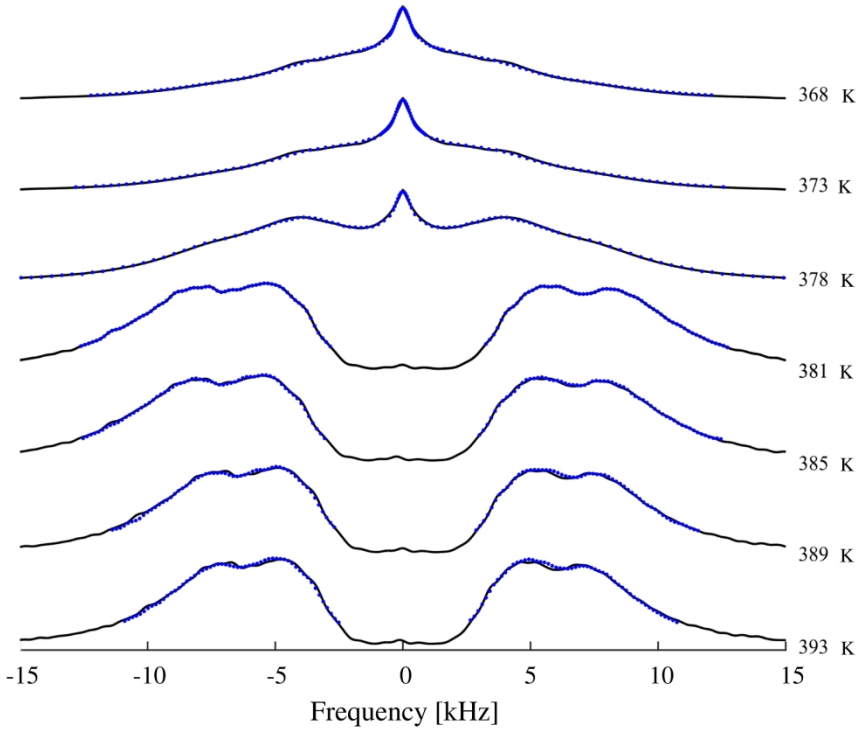

254x190mm (300 x 300 DPI)

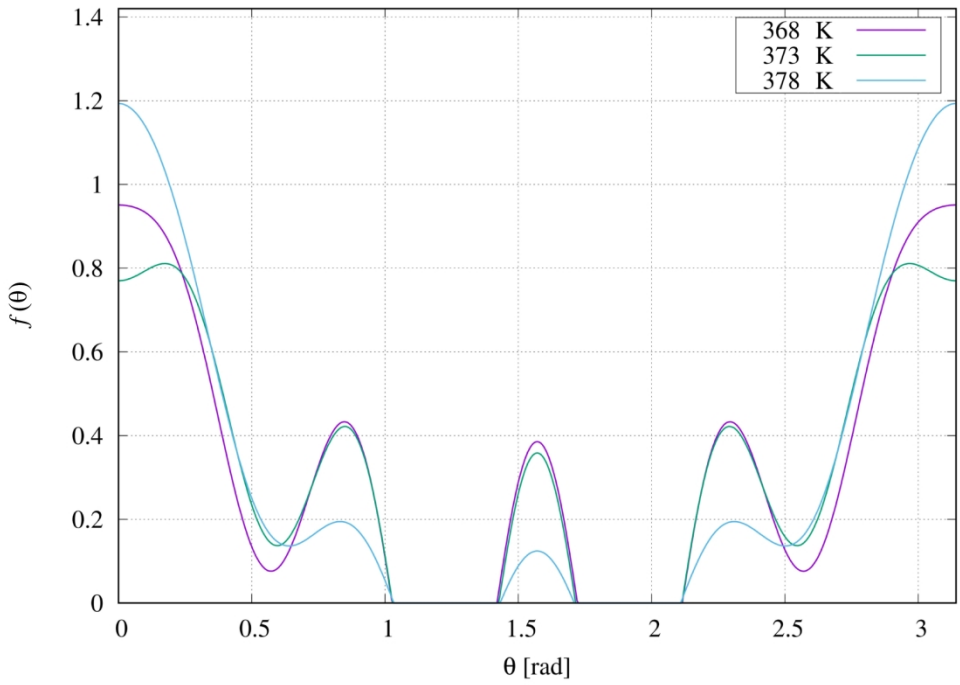

254x190mm (300 x 300 DPI)

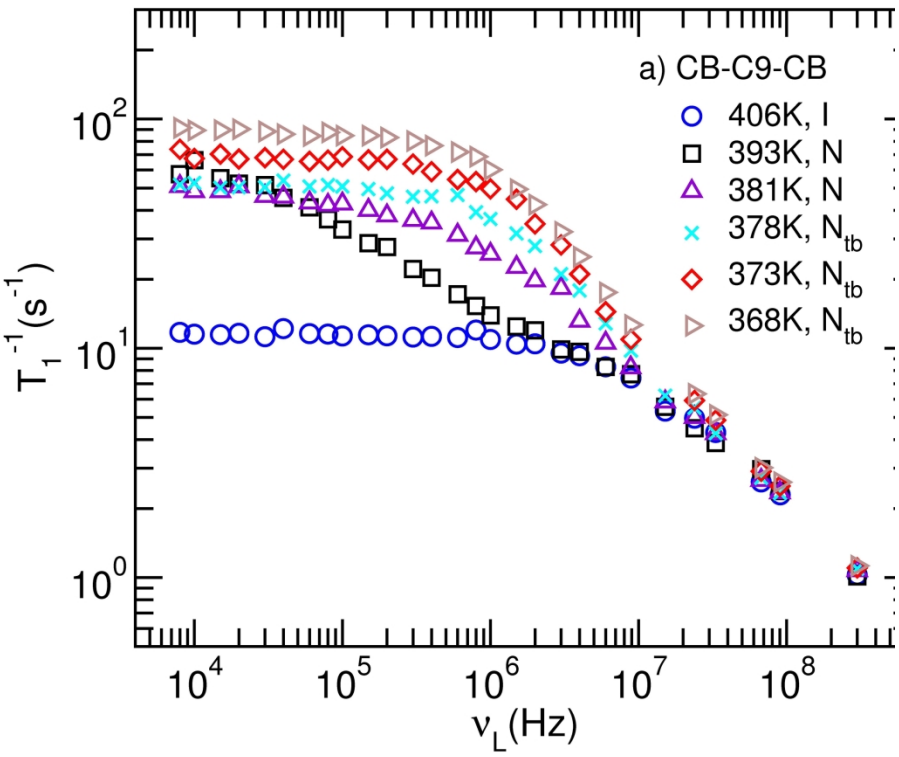

215x279mm (300 x 300 DPI)

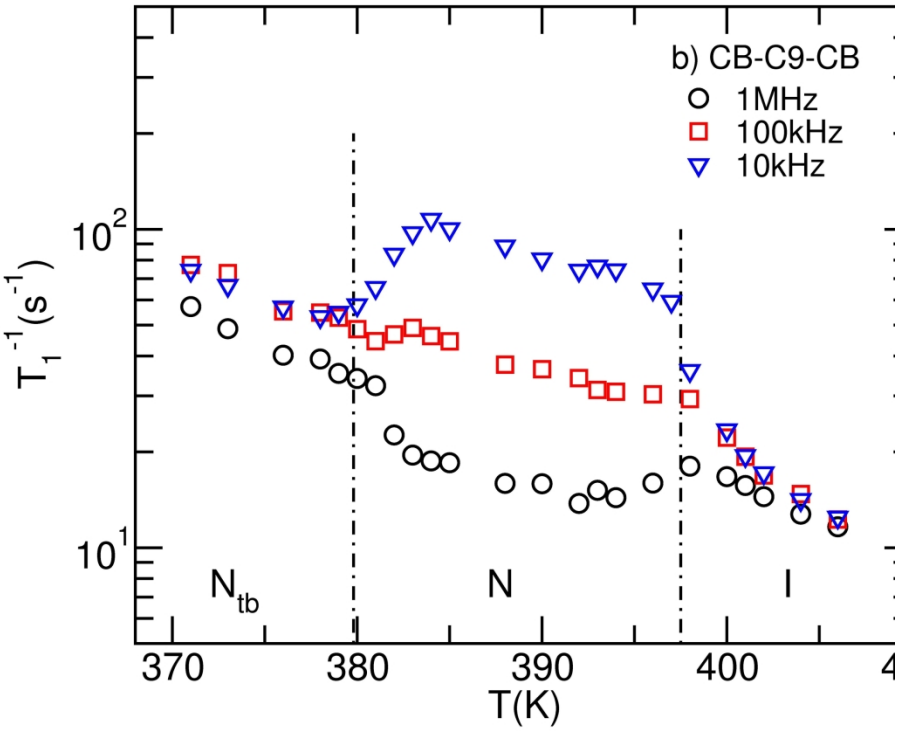

215x279mm (300 x 300 DPI)

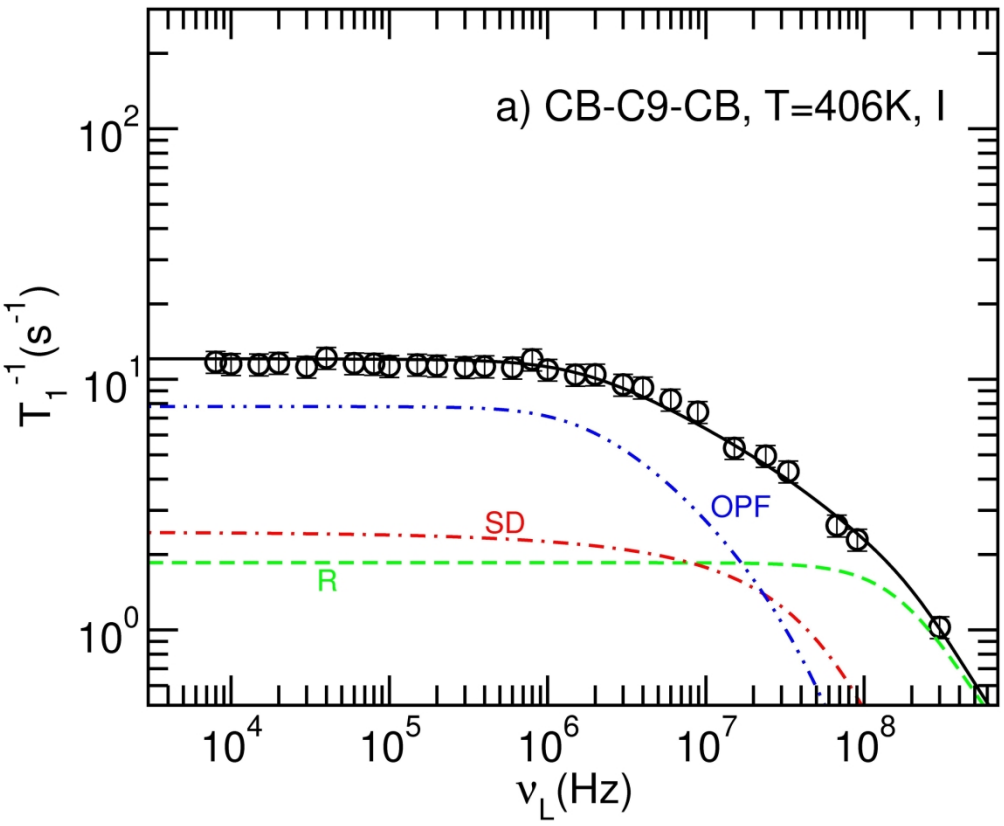

213x173mm (300 x 300 DPI)

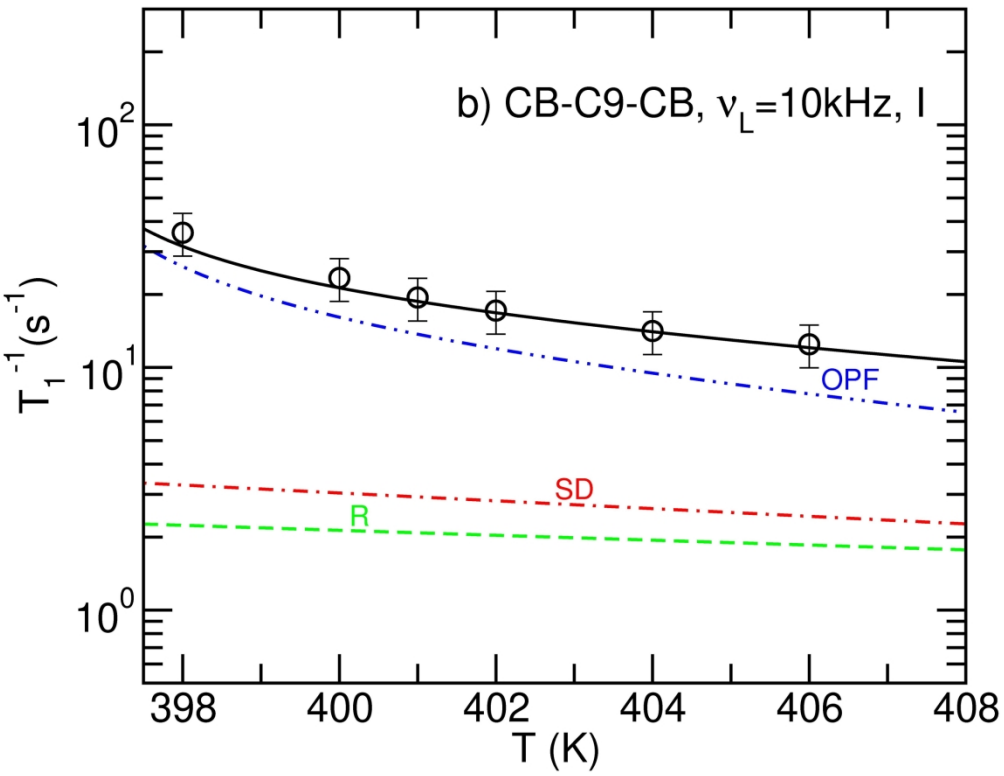

220x168mm (300 x 300 DPI)

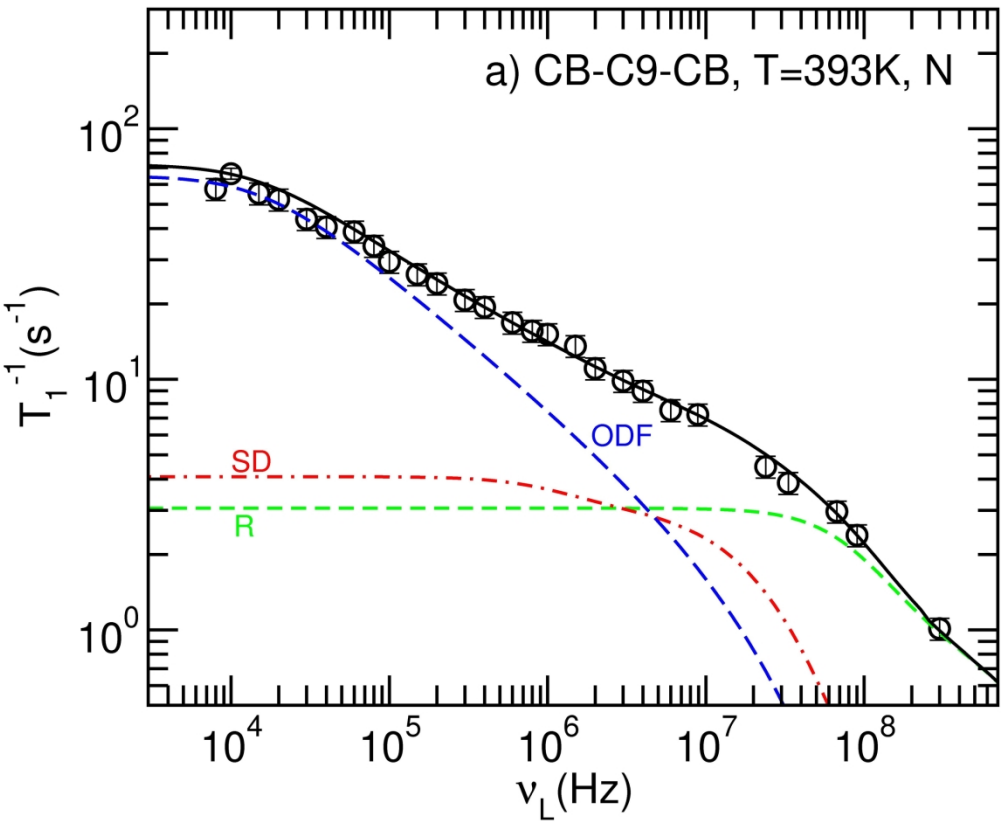

213x173mm (300 x 300 DPI)

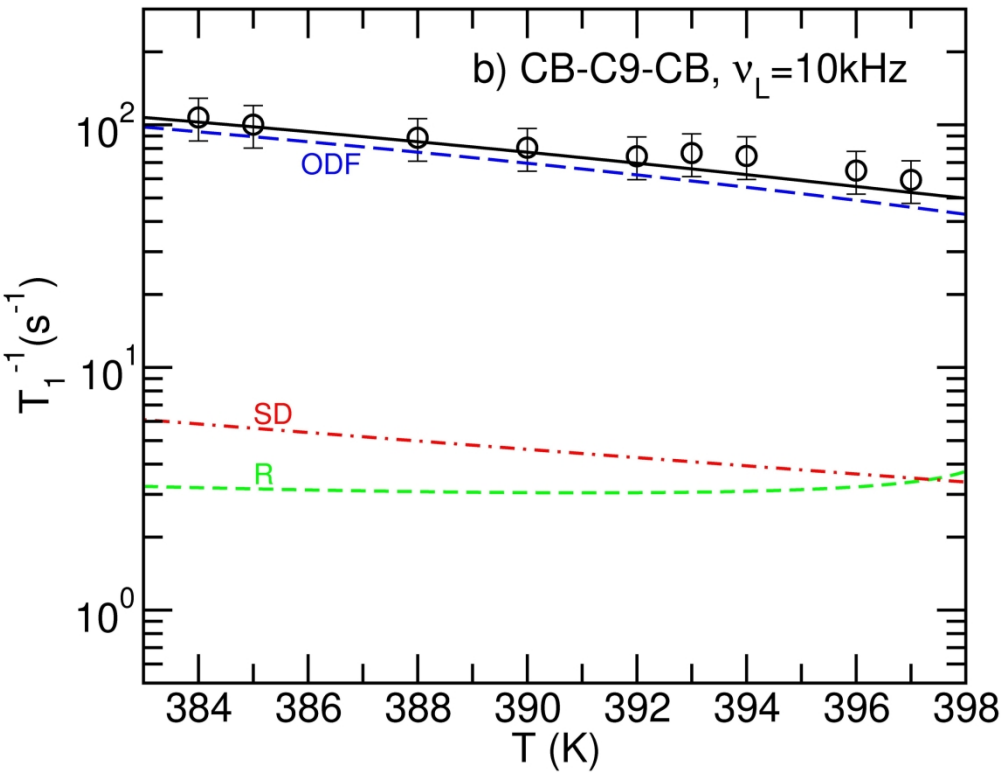

220x168mm (300 x 300 DPI)

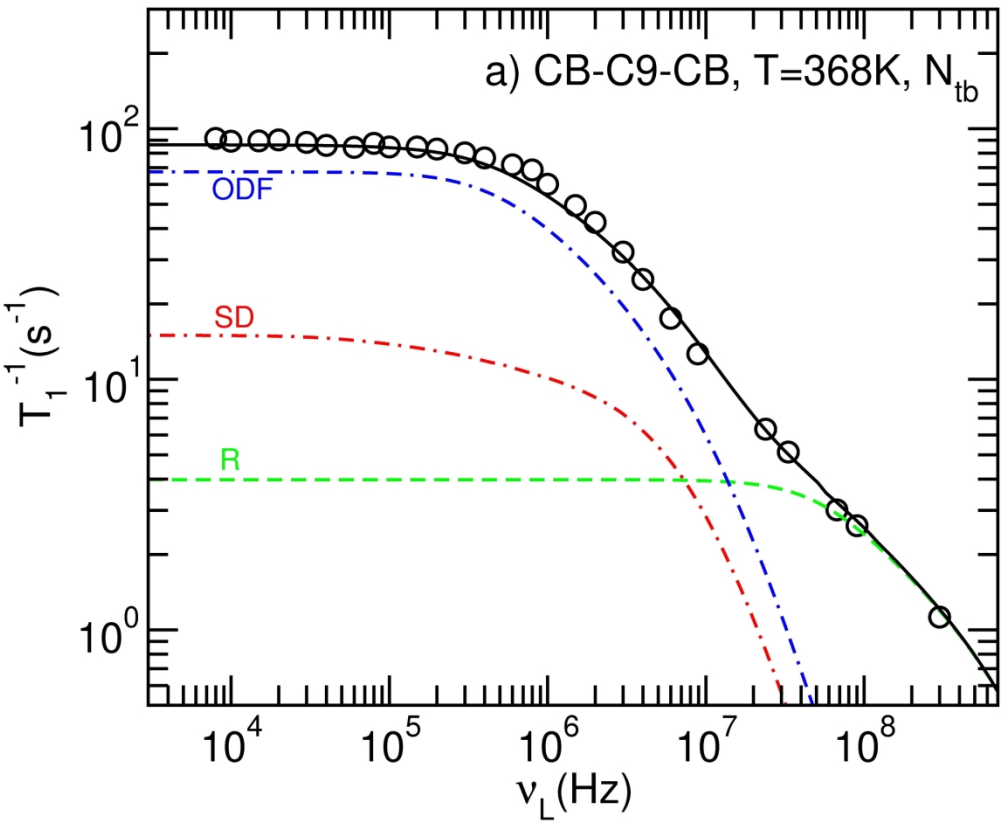

213x173mm (300 x 300 DPI)

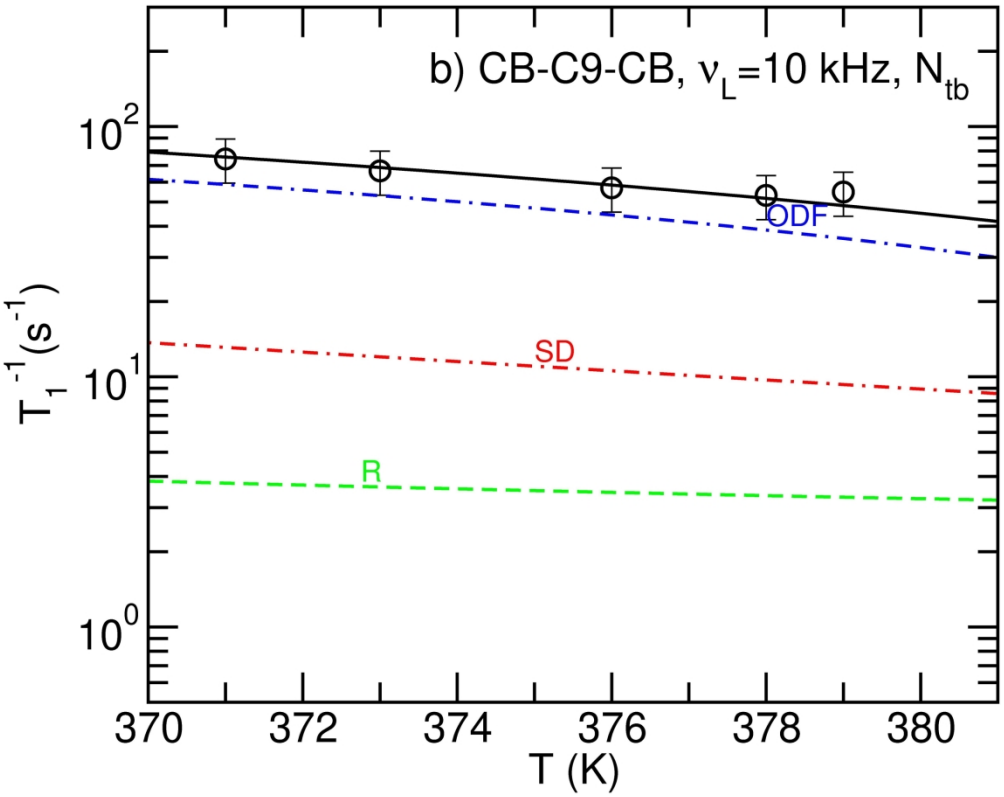

213x168mm (300 x 300 DPI)

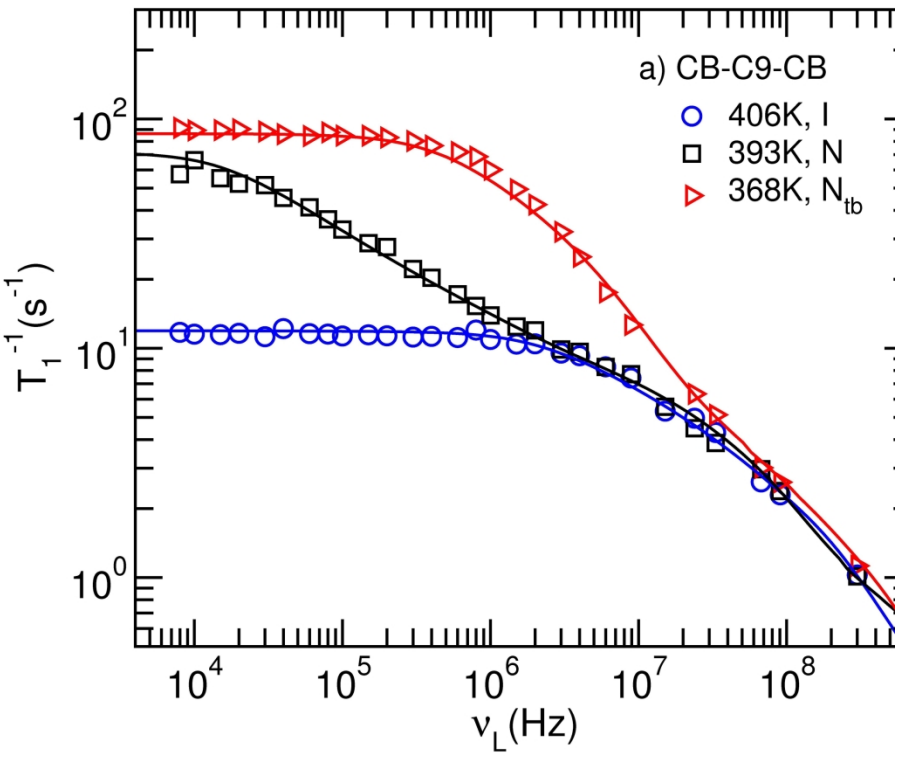

215x279mm (300 x 300 DPI)

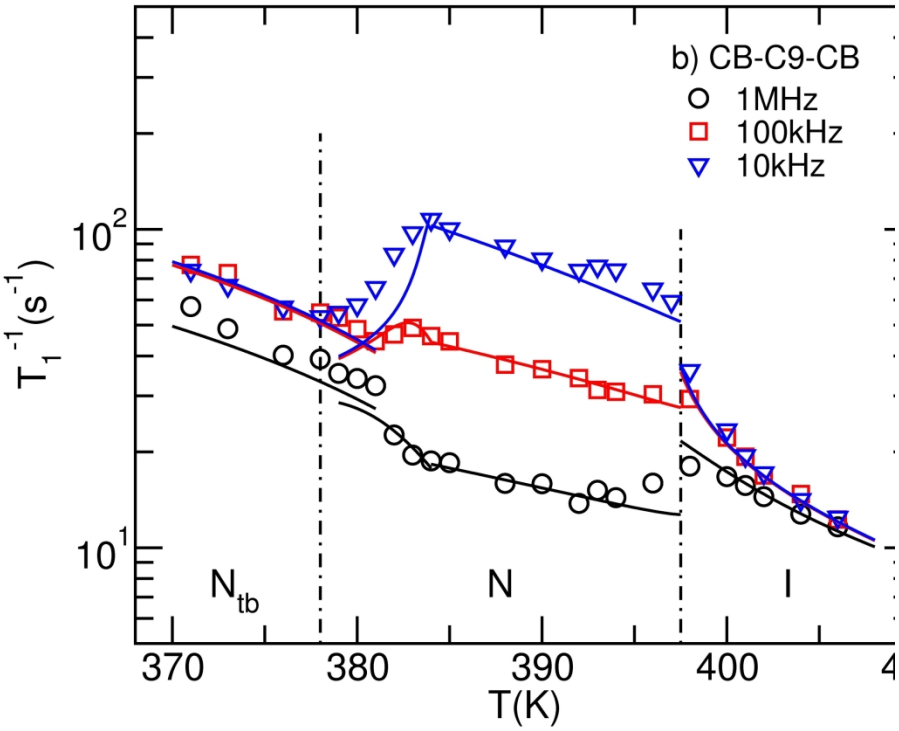

215x279mm (300 x 300 DPI)

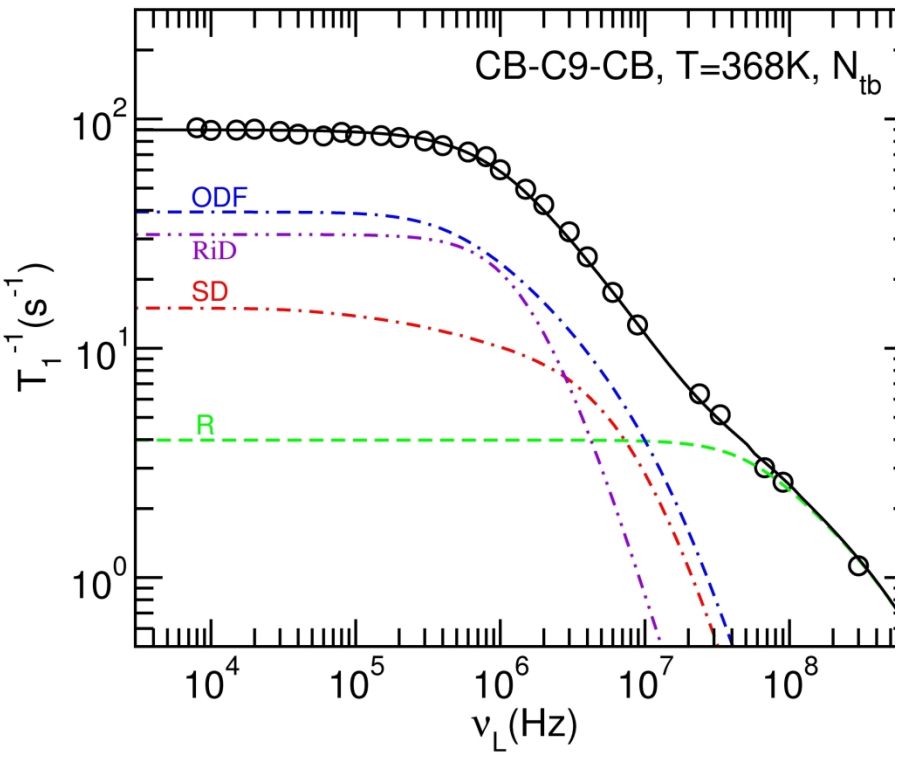

215x279mm (300 x 300 DPI)

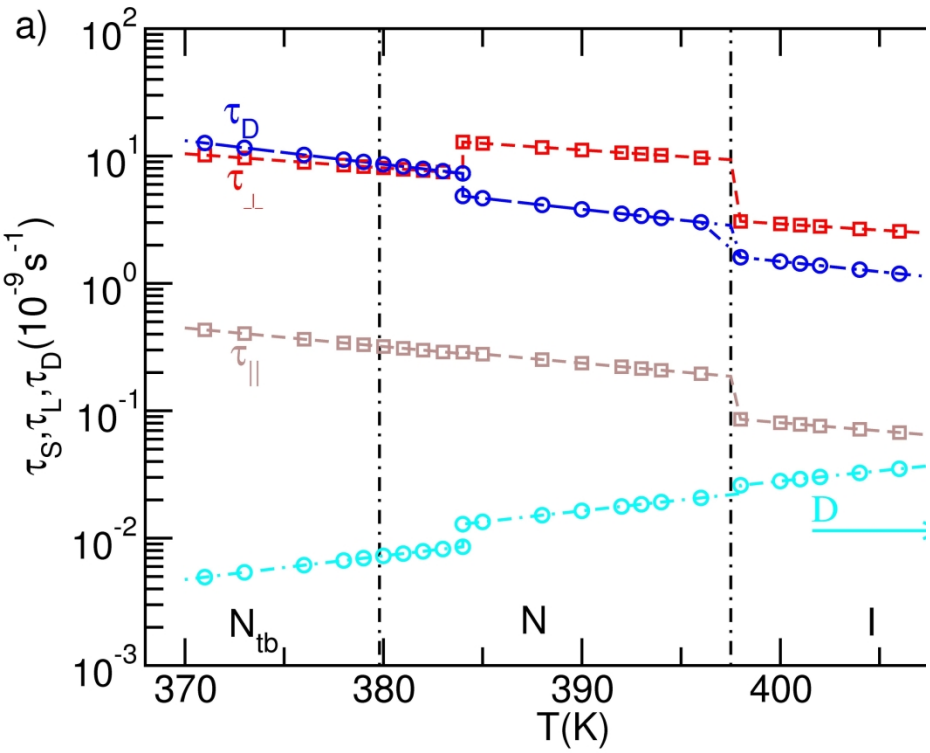

215x279mm (300 x 300 DPI)

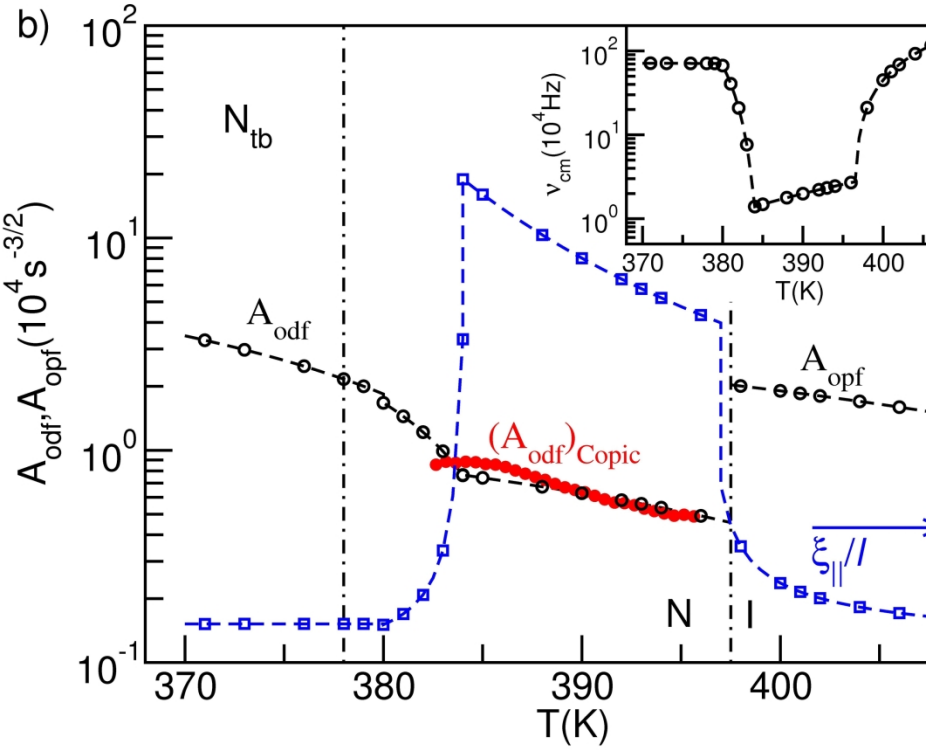

215x279mm (300 x 300 DPI)

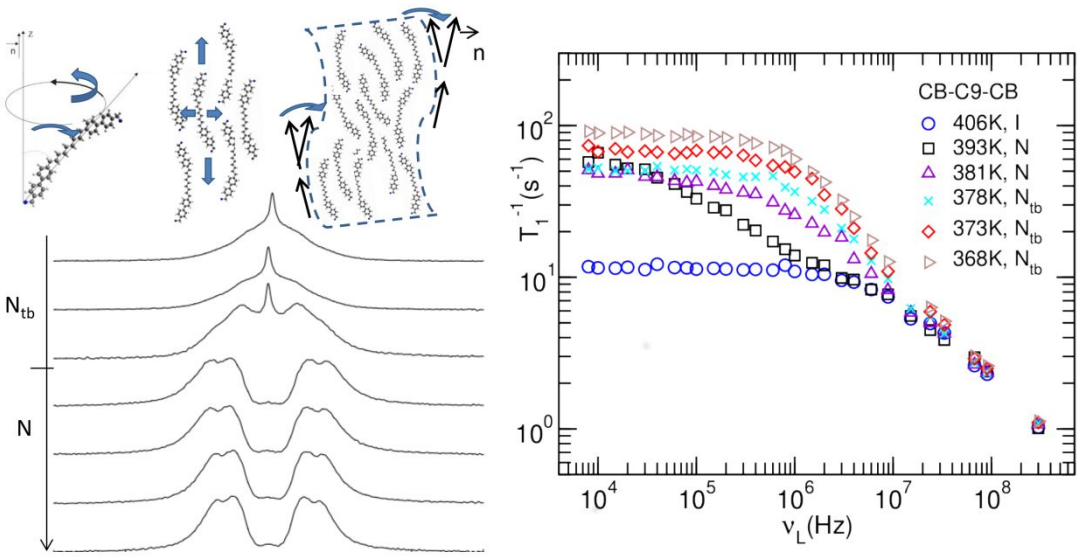

The first study combining proton NMR spectroscopy and relaxometry in the nematic and Ntb phases of the CBC9CB dimer

The first study combining proton NMR spectroscopy and relaxometry in the nematic and Ntb phases of the CBC9CB dimer

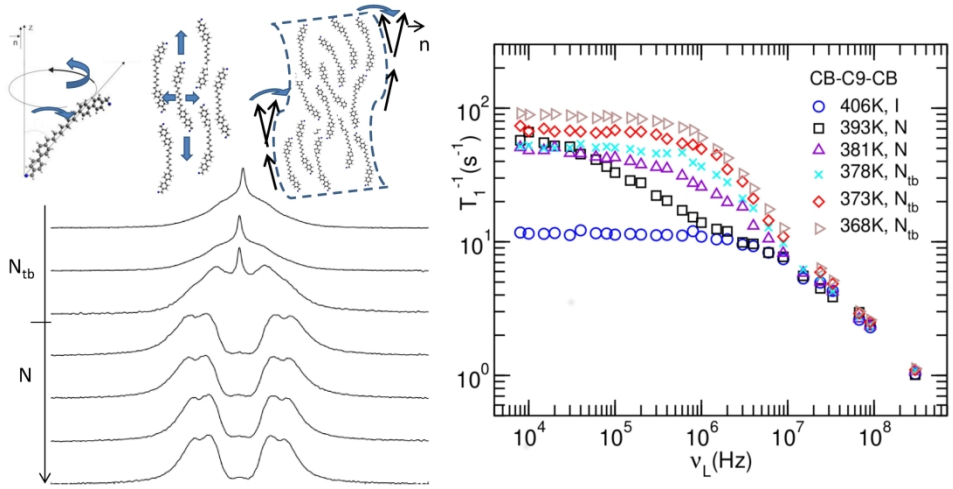

The first study combining proton NMR spectroscopy and relaxometry in the nematic and Ntb phases of the CBC9CB dimer

239x119mm (300 x 300 DPI)